

Uni-Hand: Universal Hand Motion Forecasting in Egocentric Views

Junyi Ma¹, Wentao Bao², Jingyi Xu³, Guanzhong Sun⁴, Yu Zheng¹, Erhang Zhang¹,
Xieyuanli Chen⁵, Hesheng Wang^{1*}

Abstract—Forecasting how human hands move in egocentric views is critical for applications like augmented reality, human-robot policy transfer, and service/assistive technologies. Recently, several hand trajectory prediction (HTP) methods have been developed to generate future possible hand waypoints, which still suffer from insufficient prediction targets, inherent modality gaps, entangled hand-head motion, and limited validation in downstream tasks. To address these limitations, we present Uni-Hand, a universal hand motion forecasting framework considering multi-modal input, multi-dimensional and multi-target prediction patterns, and multi-task affordances for downstream applications. We harmonize multiple modalities by vision-language fusion, global context incorporation, and task-aware text embedding injection, to forecast hand waypoints in both 2D and 3D spaces. A novel dual-branch diffusion is proposed to concurrently predict human head and hand movements, capturing their motion synergy in egocentric vision. By introducing target indicators, the prediction model can forecast the specific joint waypoints of the wrist or the fingers, besides the widely studied hand center points. In addition, we enable Uni-Hand to additionally predict hand-object interaction states (contact/separation) to facilitate downstream tasks better. As the first work to incorporate downstream task evaluation in the literature, we build novel benchmarks to assess the real-world applicability of hand motion forecasting algorithms. The experimental results on multiple publicly available datasets and our newly proposed benchmarks demonstrate that Uni-Hand achieves the state-of-the-art performance in multi-dimensional and multi-target hand motion forecasting. Extensive validation in multiple downstream tasks also presents its impressive human-robot policy transfer to enable robotic manipulation, and effective feature enhancement for action anticipation/recognition. We will release our code, pretrained models of Uni-Hand, and novel benchmarks at the project page: <https://irmvlab.github.io/unihand.github.io>.

Index Terms—Hand Motion Forecasting, Hand Trajectory Prediction, Egocentric Vision, Diffusion Models

1 INTRODUCTION

Predicting human behaviors over future time horizons is critical for applications such as augmented reality and human-robot interaction. As an important interface for human-environment interaction, the human hand offers valuable motion knowledge that facilitates various downstream tasks in embodied intelligence [1], [2], [3], [4]. However, despite significant progress in other human behavior anticipation tasks like predicting gaze locations [5], [6], [7], [8], and interaction regions [9], [10], [11], forecasting fine-grained human hand motion still remains challenging. To align better with hand movement patterns and potential intentions from a human perspective, some egocentric-vision-only hand motion forecasting (HMF) approaches [12], [13], [14], [15] have been developed in recent years. They receive past human egocentric (first-person) observations and directly predict future hand trajectories in the specified reference frame. However, these methods exhibit significant limitations that hinder their further performance improvement and effectiveness in possible downstream applications:

¹Junyi Ma, Yu Zheng, Erhang Zhang, and Hesheng Wang are with IRMV Lab, the Department of Automation, Shanghai Jiao Tong University.

²Wentao Bao is with Meta Reality Labs.

³Jingyi Xu is with the Department of Electronic Engineering, Shanghai Jiao Tong University.

⁴Guanzhong Sun is with the School of Information and Control Engineering, China University of Mining and Technology.

⁵Xieyuanli Chen is with the College of Intelligence Science and Technology, National University of Defense Technology.

*Corresponding author emails: wanghesheng@sjtu.edu.cn

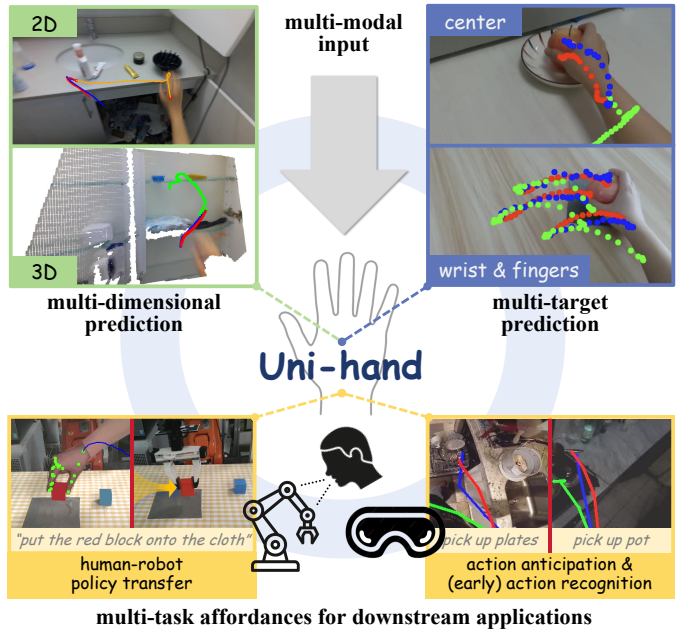


Fig. 1: Uni-Hand is a universal hand motion forecasting framework which facilitates multi-dimensional and multi-target predictions with multi-modal input. It also enables multi-task affordances for downstream applications.

- **Insufficient prediction targets:** The existing hand motion forecasting paradigms exclusively concentrate on the generation of future hand centers (of the potential bounding

boxes) as target motion waypoints [14], [15], [16]. Despite its necessity for providing hand movement trends, these methods basically overlook how different joints of the fingers and wrist move in 2D and 3D spaces. Besides, they do not involve locating the precise timings when the hand will make contact with and separate from target objects. Therefore, there is a lack of sufficient motion knowledge in future time horizons for practical deployments, such as human-robot manipulation policy transfer.

- **Modality gaps:** The current HMF paradigms are only designed to process 2D egocentric video inputs, without incorporating 3D structure awareness. As humans leverage stereo vision for 3D spatial understanding during interactions, the inherent discrepancy between the current 2D inputs and 3D perceptions inevitably creates a gap between predicted hand trajectories and real hand movements. In addition, the absence of textual modality interfaces prevents explicitly incorporating known human intentions or instructions. It also exacerbates the discrepancy between the HMF model optimization and possible deployments in language-conditioned downstream tasks.
- **Entangled hand-head motion:** Human hand motion is closely linked to whole-body kinematics, where the head movement is its most straightforward concurrent motion to provide visual observations. Understanding how the head moves benefits hand motion forecasting [17], [15]. Although some recent works [15], [16], [17] have attended to encode *past* headset camera egomotion into the hand state transition model, they still fail to explicitly decouple the prediction of entangled hand and head motion in *future* time horizons. This impairs the prediction models' ability to comprehend future hand motion patterns in the egocentric view of incoming hand-head cooperation.
- **Limited validation in downstream tasks:** The existing HMF frameworks aim to reduce the errors between predicted waypoints and ground-truth human demonstrations. While this objective is well-justified, their capability to support downstream tasks should be further analyzed in this literature. Transferring human actions to robot manipulation has captured substantial attention nowadays, owing to the naturalistic hand-object interaction patterns and high accessibility of human demonstrations [18]. Therefore, evaluating the transferability of HMF models to robotic manipulation tasks warrants significant research attention. In addition, hand motion patterns and action categories are strongly correlated. However, how predicted hand motion features facilitate downstream action category anticipation, early action recognition, and action recognition still remains unexplored.

To address the above-mentioned limitations, we propose a universal hand motion forecasting framework, dubbed *Uni-Hand*. *Uni-Hand* absorbs multi-modal inputs to achieve multi-dimension/-target hand motion prediction, and effectively provides multi-task affordances for downstream applications. **To extend the prediction targets**, *Uni-Hand* introduces target indicators in denoising diffusion to forecast hand centers or specified joints in both 2D and 3D space. It also integrates an additional interaction state decoder to locate the timings of hand-object contact and separation events. We therefore present a more flexible HMF solution

compared to the existing paradigms [13], [15], [17] that only attend to hand center prediction. **To narrow the modality gaps**, we incorporate multiple modalities as the inputs including 2D RGB images, 3D point clouds, past hand waypoints, and text prompts. This not only enhances the awareness of 3D structure information in our framework, but also provides a textual modality interface for integrating possible language instructions in real-world robotic applications. **To solve the problem of entangled hand-head motion**, we design a dual-branch diffusion to concurrently forecast head and hand movements, explicitly capturing their synergy for more accurate HMF. Ultimately, **for extensive validation in downstream tasks**, we deploy our proposed framework on multiple real-world robotic tasks, validating its capability to facilitate atomic skills, language-conditioned implementations, and long-horizon tasks. We also demonstrate its affordable motion features to improve the off-the-shelf framework for conventional action anticipation, early action recognition, and action recognition tasks.

In summary, the **main contributions** of this paper are fourfold:

- **Universal HMF framework:** We present *Uni-Hand*, a universal hand motion forecasting framework, featuring a versatile solution for multi-dimension/-target HMF and multi-task affordances for downstream applications.
- **Dual-branch diffusion:** We propose a novel dual-branch diffusion, which employs multi-modal information as input to concurrently predict future headset camera egomotion and hand movements in egocentric views.
- **Hybrid Mamba-Transformer denoising:** A novel hybrid Mamba-Transformer module is designed for denoising hand motion latents. It combines the strong temporal modeling ability of Mamba and the global context-awareness of Transformer to harmonize multi-modal features. We also inject text embeddings into the hybrid module to facilitate language-conditioned tasks.
- **HMF benchmark:** To the best of our knowledge, this is the first HMF research considering the assessment of hand forecasting algorithms' effectiveness in enabling downstream tasks, including robotic manipulation, action anticipation, early action recognition, and action recognition. The comprehensive experiments on multiple publicly available datasets and our newly proposed benchmarks demonstrate that *Uni-Hand* achieves SOTA performance on 2D/3D hand motion forecasting, and can effectively adapt to the downstream tasks.

This work is an extension of the preliminary version [19], in which we only explored how to harmonize multiple input modalities for hand center prediction and achieve decoupling hand-head motion forecasting. In this study, we substantially expand in the following ways:

- We extend the original 3D prediction paradigm to a universal framework for multi-dimension/-target HMF and multi-task affordances for downstream applications.
- We incorporate additional prediction targets besides hand centers, encompassing multiple hand joints and interaction states (contact/separation).
- A new textual modality interface (text embedding injection) is designed to enhance our model's awareness of specific task instructions.

- A comprehensive extension of experiments on public datasets and our new benchmarks presents the model’s foundation capability to facilitate downstream tasks including real-world robotic manipulation, action anticipation, early action recognition, and action recognition.

This paper is organized as follows. Sec. 2 reviews the related works in literature. Sec. 3 details the design of our proposed Uni-Hand and its training/inference scheme. Sec. 4 showcases the extensive experimental results quantitatively and qualitatively. Ultimately, Sec. 5 concludes the paper and provides our insights.

2 RELATED WORK

2.1 Hand Trajectory Prediction in Egocentric Vision

Hand trajectory prediction (HTP) is a key component in understanding future hand motion patterns. Given sequential egocentric observations, HTP aims to forecast future possible hand waypoints in the 2D image plane or 3D space. Here, the hand waypoints denote the bounding box centers of detected hands. Motivated by the need for enhanced scaling capabilities, some 2D HTP approaches have been pioneeringly developed based on a large volume of human activity videos. For example, OCT [13] uses a Transformer [20] based encoder-decoder architecture to jointly predict hand waypoints and object hotspots. In contrast, Diff-IP2D [15] replaces the Transformer blocks in OCT with egomotion-aware diffusion models, achieving better 2D HTP performance. Similar to Diff-IP2D, EMAG [17] also innovatively encodes homography matrices of camera egomotion into 2D hand trajectory prediction with the cross-attention mechanism. These two works make initial efforts to integrate headset camera egomotion awareness into the 2D HTP pipeline. To further enhance the model’s interpretability regarding fused camera egomotion, MADiff [16] incorporates Mamba [21] to model sequential hand state transition, based on a new motion-driven selective scan. Its powerful egomotion-aware Mamba block is out-of-the-box with respect to 2D predictive tasks in first-person views. More recently, HandsOnVLM [22] introduces a VLM scheme to transform 2D HTP into a VQA-style task. To further validate the applicability in real-world scenes, Bahl *et al.* [23] build an affordance model referencing OCT [13] and deploy it in robotic applications like offline data collection and reward-free exploration.

Although 2D HTP is more scalable due to the availability of internet-scale human activity videos [16], predicting in 3D space yields more human-intent-aligned results. For instance, USST [14] receives 2D image prompts to directly generate future 3D hand waypoints by autoregressive Transformers. EgoH4 [24] extends 3D HTP to body pose estimation, which can predict locations of invisible hands. In contrast to EgoH4 which focuses on whole body movements, our recent MMTwin [19] attends to the most critical body part, i.e., the head and hand, in hand-object interaction, forecasting their future motion concurrently. Compared to egomotion-aware 2D HTP [15], [17], [16] that only encodes past head motion, MMTwin builds an additional diffusion branch to predict future head motion latents.

Despite the significant progress in the above-mentioned 2D and 3D hand trajectory prediction, these methods ba-

sically only determine future centers of potential hand bounding boxes. However, the hand center constitutes an excessively coarse-grained prediction target, incapable of representing hand pose variations. This hinders fine-grained understanding of human behavior in hand-object interaction. Besides, these methods are agnostic to the potential timings of hand-object contact and separation. Therefore, they cannot be easily transferred to downstream tasks such as robot manipulation, since trajectories can only determine “where to move” rather than “when to grasp”. In contrast, Uni-Hand proposed in this work can forecast future 2D and 3D positions of multiple hand joints besides center points, leading to awareness of hand pose changes in egocentric views. We introduce target indicators to let the denoising diffusion model distinguish different prediction targets. Moreover, we develop an additional decoder to forecast future interaction states, which can determine the hand-object contact/separation periods. Thus, Uni-Hand extends the conventional HTP literature to more informative hand motion forecasting by enriching prediction targets, and can practically facilitate multiple downstream applications.

2.2 Diffusion Models in Hand Motion Analysis

In recent years, hand motion analysis has attracted much attention due to the informational richness of hand-centric data for downstream tasks. While object-agnostic hand mesh recovery [25], [26], [27], [28] and object-aware 3D HOI reconstruction [29], [30], [31], [32] have witnessed significant advances, synthesizing reasonable hand poses around target objects and analyzing hand dynamics along the time axis are more challenging. With the advent of diffusion models [33], [34], some works such as HOIDiffusion [35], Gears [36], and DiffH2O [37] seamlessly integrate the powerful generation ability of diffusion models to generate hand meshes from scratch. However, they basically underestimate how the hand approaches the target object. More recently, PEAR [38] considers analyzing the hand motion trend during the interaction process. In contrast to PEAR, Tang *et al.* [39] develop a prompt-based future-driven diffusion model for predicting future 3D coordinates of multiple hand joints. Despite being more fine-grained, this method does not attend to wide-range wrist movements. Conversely, Diff-IP2D [15] and MADiff [16] both utilize DiffuSeq [40]-style models to forecast future wide-range hand movements, but lose detailed joint motion as mentioned before.

This work also adapts the advanced generation ability of diffusion models, to achieve multi-dimensional and multi-target future hand motion forecasting. Unlike the existing diffusion-based schemes, we propose a novel hybrid Mamba-Transformer architecture as the denoising model to harmonize multi-modal input. Besides, we introduce camera egomotion analysis within the dual-branch diffusion to enable more comprehensive hand motion understanding.

2.3 Downstream Tasks of Hand Motion Forecasting

As hands are fundamental to physical interaction in human daily life, they have driven growing research interest in human-robot policy transfer for manipulation tasks. Traditional imitation learning [41], [42] techniques rely on costly teleoperation and lack cross-embodiment generalization. In contrast, widely available human videos already

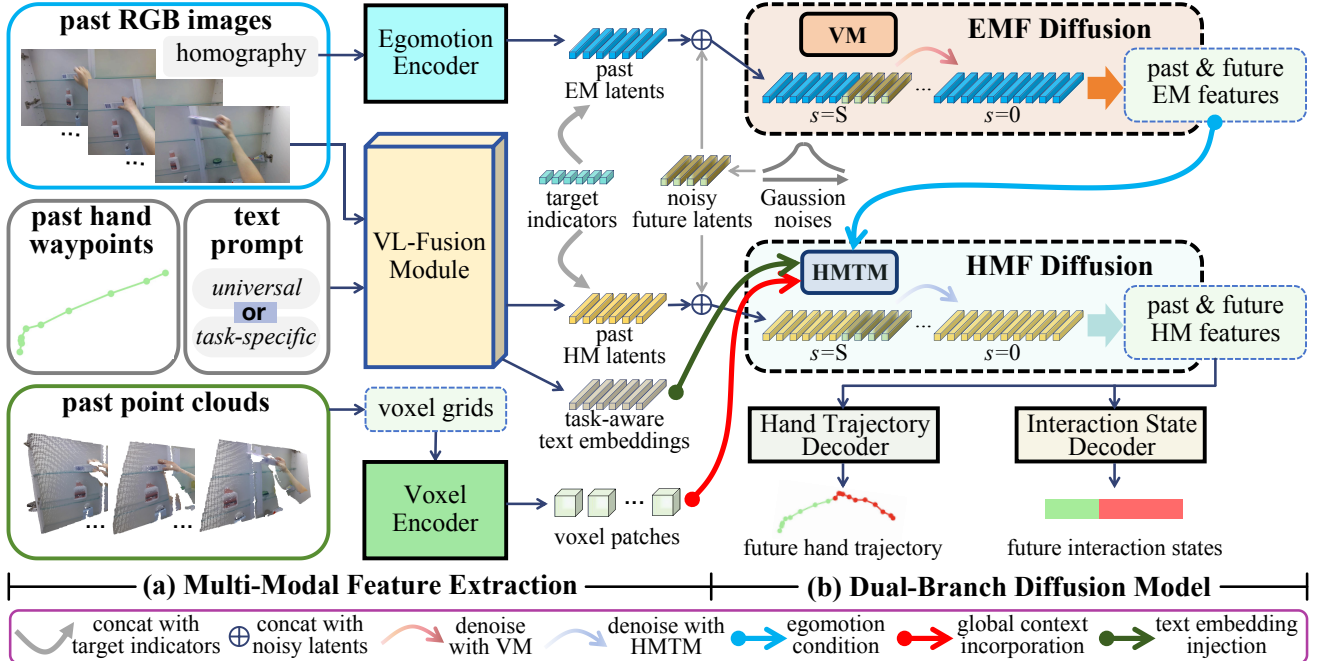


Fig. 2: System overview of Uni-Hand. Uni-Hand (a) converts multi-modal input into latent feature spaces, and (b) decouples predictions of future egomotion latents (EM latents) and hand motion latents (HM latents) by a novel dual diffusion. The vanilla Mamba (VM) is used for denoising in the ego-motion-forecasting diffusion (EMF diffusion). We further design a new denoising model in hand-motion-forecasting diffusion (HMF diffusion) with a hybrid Mamba-Transformer module (HMTM). The predicted HM latents are ultimately decoded to future hand trajectories and interaction states.

contain rich demonstrations. They are robot-agnostic and offer transferable knowledge for manipulation. Therefore, directly capturing human hand motion data from egocentric or exocentric videos to guide robot policy generation is a promising path towards embodied intelligence. Compared to producing pretrained visual representations from large-scale human videos [43], [44], [45], [46], extracting explicit affordances related to human hands enables more straightforward human-robot policy transfer. For example, OKAMI [47] retargets the body motions and hand poses separately from a single video imitation to humanoid robot actions. Following OKAMI using only one video demonstration, YOTO [48] proposes a proliferating strategy for one-shot teaching, enabling more demonstrations for the bimodal diffusion policy. Instead of relying entirely on human video data, Motion Tracks [49] combines robot and human video demonstrations to train a motion prediction network. Compared to these imitation learning schemes, ManipTrans [18] models the transfer process with reinforcement learning. Wen *et al.* [50] design a two-stage framework for any-point trajectory modeling, which guides policy learning with predicted future point trajectories. More recently, Qiu *et al.* [1] unify the state-action space of humanoid embodiments and human hands for action prediction.

Inspired by these human-robot transfer strategies, in this work, we expand the existing HMF assessment paradigm [12], [13], [15] by evaluating Uni-Hand’s capability to support robot manipulation tasks. That is, we directly use pretrained Uni-Hand to generate executable trajectories and gripper actions for a real robot. The success rates of multiple manipulation tasks highlight its potential for real-world downstream deployments. In addition, we also present whether Uni-Hand can benefit the other three

critical downstream tasks in egocentric vision, i.e., action anticipation [51], [52], [53], [54], early action recognition [55], [56], [54], and action recognition [57], [58], [59], [60], [54]. The improvement of anticipation and recognition accuracy by introducing hand motion features shows Uni-Hand’s applicability in possible wearable assistive technologies.

3 PROPOSED METHOD

3.1 System Overview

Here we first provide the overall inference pipeline of Uni-Hand in Fig. 2. Given a sequence of past egocentric observations $\mathcal{O} = \{O_t\}_{t=-N_p+1}^0$, past waypoints of the hand center or a specific joint $\mathcal{H}_p = \{H_t\}_{t=-N_p+1}^0 (H_t \in \mathbb{R}^2 \text{ or } \mathbb{R}^3)$, and a text prompt L , our proposed Uni-Hand aims to predict future hand trajectories $\mathcal{H}_f = \{H_t\}_{t=1}^{N_f} (H_t \in \mathbb{R}^2 \text{ or } \mathbb{R}^3)$, as well as interaction states $\mathcal{G}^f = \{G_t\}_{t=1}^{N_f} (G_t \in \{0, 1\})$ if needed. N_p and N_f denote the number of frames in the past and future time horizons. Each observation O_t consists of an egocentric 2D RGB image $I_t \in \mathbb{R}^{c \times h \times w}$ and 3D point clouds $D_t \in \mathbb{R}^{n \times 3}$. The temporal interaction state $G_t = 0$ indicates that the hand and target object are physically separated, while $G_t = 1$ represents that they are in contact. Following the previous works [13], [14], [15], we forecast the future hand waypoints on a fixed reference frame (e.g., the image plane and the camera coordinate system of the first frame O_{-N_p+1} for 2D and 3D HMF tasks, respectively). As can be noted, our framework absorbs multi-modal information to enhance the prediction model’s perceptual capability of environments and tasks, compared to the current baselines [12], [13], [15], [17] only using image inputs. Besides, UniHand can also predict waypoints for multiple joints (e.g.,

\mathcal{H}_f^{j0} , \mathcal{H}_f^{j4} , and \mathcal{H}_f^{j8}) in parallel since the data from different joints can be packed into a single batch.

Specifically, we first extract features/latents from the input RGB images, hand waypoints, and text prompt (Fig. 2(a), Sec. 3.2). The VL-fusion module generates hand motion latents (HM latents) by fusing vision-language features, waypoint features, task-aware text embeddings, and target indicators. The egomotion encoder computes sequential homography matrices of the input image sequence as headset camera egomotion, and then encodes them to egomotion latents (EM latents). To integrate 3D structure features, the voxel encoder converts the past point clouds to voxel patches. Subsequently, a dual-branch diffusion model (Fig. 2(b), Sec. 3.3), encompassing hand-motion-forecasting diffusion (HMF diffusion) and ego-motion-forecasting diffusion (EMF diffusion), is tailored for concurrently predicting future HM latents and EM latents conditioned on their past counterparts. The EMF diffusion uses the vanilla Mamba to efficiently denoise the noisy future latents. In contrast, the HMF diffusion adopts our hybrid Mamba-Transformer module as the denoising model, which consists of stacked egomotion-aware Mamba blocks and structure-aware/task-aware Transformer. It harmonizes hand motion modeling for egocentric vision, text embedding injection for task-aware optimization, and global context incorporation for 3D structure awareness. Ultimately, the denoised future HM latents are decoded to future hand trajectories and interaction states. We train the components of our Uni-Hand in an end-to-end manner with multiple loss functions (Sec. 3.4).

3.2 Multi-Modal Feature Extraction

3.2.1 Egomotion Encoder

Since our proposed framework considers modeling head motion in hand motion forecasting, we first calculate sequential homography $\mathcal{M} = \{M_t\}_{t=-N_p+1}^0$ ($M_t \in \mathbb{R}^{3 \times 3}$) from I_t to represent past headset camera egomotion following [15], [17]. M_t denotes the homography matrix between t th frame and the first frame ($t = -N_p + 1$) estimated by SIFT descriptors [61] with RANSAC [62]. Subsequently, the egomotion encoder, composed of MLPs, encodes egomotion homography \mathcal{M} to past egomotion features $F_p^{\text{em}} \in \mathbb{R}^{N_p \times f}$ as latents for the following EMF diffusion. Note that the ground-truth (GT) future EM latents $F_f^{\text{em}} \in \mathbb{R}^{N_f \times f}$ only exist in the training process for supervision and will be replaced by sampled noises $F_{\text{noise}}^{\text{em}} \in \mathbb{R}^{N_f \times f}$ to enable denoising-based inference in EMF diffusion as shown in Fig. 2(a).

3.2.2 VL-Fusion Module

For hand motion forecasting, we develop the VL-fusion module to generate HM latents by fusing multiple modalities, including RGB images, past waypoints, and text prompts. As shown in Fig. 3, here we support two types of text prompting for different HMF applications, the universal prompt and the task-specific instruction. When the target hand motion is task-agnostic, we advocate using the universal prompt “*hand*” to generate vision-language fusion features $X^{\text{vl}} \in \mathbb{R}^{(N_p+\ell) \times x}$ by the pretrained GLIP [63] following [16]. x is the feature channel dimension. ℓ equals N_f during training, and is set to 0 during inference since future HM latents will be replaced by sampled noises in

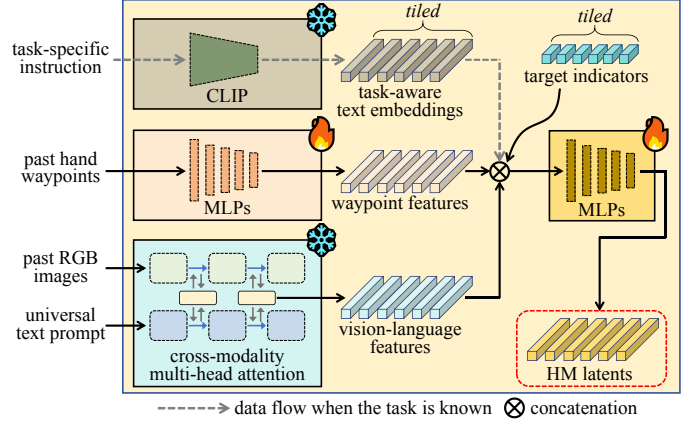


Fig. 3: Architecture of the VL-fusion module. It generates HM latents for the following HMF diffusion by fusing vision-language features, waypoint features, and task-aware text embeddings.

the inference process of our HMF diffusion. The universal text prompt helps to semi-implicitly capture hand poses and hand-scenario relationships within each image through GLIP’s deepest cross-modality multi-head attention. Conversely, once the task being performed by the hand is known, an additional task-specific instruction (e.g., “*push the block onto the cloth*”) is absorbed by the VL-fusion module to generate the text embedding $X^{\text{task}} \in \mathbb{R}^x$ with CLIP [64] for task-awareness in hand motion forecasting.

Moreover, we use MLPs to encode past hand waypoints to waypoint features $X^{\text{wp}} \in \mathbb{R}^{(N_p+\ell) \times x}$, which are further concatenated with X^{vl} and tiled X^{task} . As showcased in Fig. 3, the additional target indicators are further concatenated with them to designate the prediction target. The target indicators consist of the tiled one-hot embeddings $X^{\text{tar}} \in \mathbb{R}^e$, where e denotes the total number of prediction targets. Ultimately, the feature combos are fused by MLPs to produce the HM latents $F_p^{\text{hm}} \in \mathbb{R}^{N_p \times f}$ and $F_f^{\text{hm}} \in \mathbb{R}^{N_f \times f}$ for the following HMF diffusion. f represents the channel dimension of HM latents. F_f^{hm} only exists in the training stage for reconstruction supervision since noisy future latents $F_{\text{noise}}^{\text{hm}} \in \mathbb{R}^{N_f \times f}$ is concatenated to F_p^{hm} in the inference stage of the HMF diffusion. By seamlessly integrating the target indicators into the framework, Uni-Hand identifies HM latents of different hand centers and joints, and achieves multi-target forecasting with the following HMF diffusion.

3.2.3 Voxel Encoder

Point Cloud Preprocessing. Uni-Hand advances 3D structure-awareness by absorbing point cloud observations for more reasonable HMF compared to the existing methods which only receive RGB images. The headset RGB-D camera captures a depth image aligned with its RGB counterpart I_t , which is directly transformed to the input point cloud $D_t \in O_t$ for Uni-Hand. To address the practical constraints of computational efficiency and memory requirements, we convert the holistic point cloud into a more compact voxelized form, as shown in Fig. 4. Specifically, we first exploit MobileSAM [65] to remove depth points projected to arms for each D_t . This is because arm movements generate artifact points hindering global 3D representation accuracy during the following multi-frame aggregation. Subsequently, all

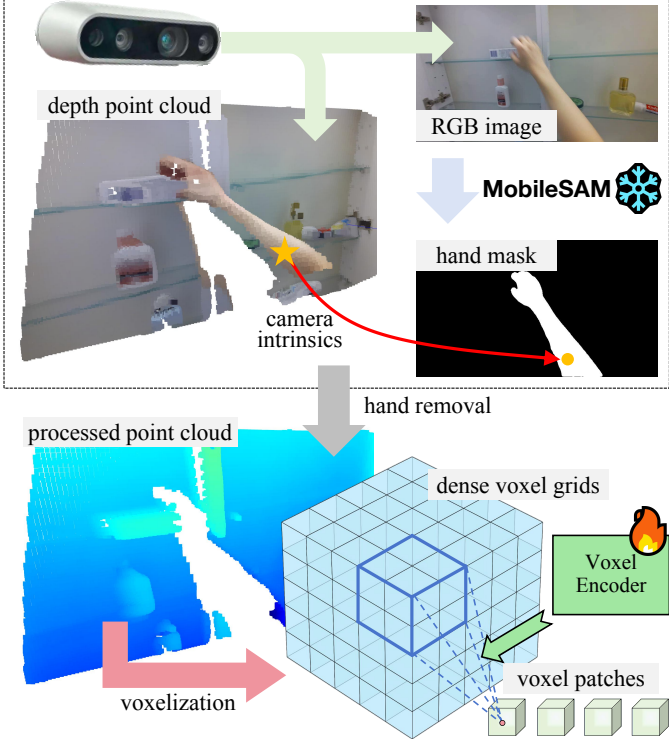


Fig. 4: Hand removal for purified point clouds. We regard the voxel patches encoded by the voxel encoder as 3D global context for the denoising process in the HMF diffusion.

the purified point clouds within the past egocentric observations \mathcal{O} are transformed into a unified global coordinate system by visual odometry. Then we aggregate them into voxel grids to avoid disturbance of the unordered point cloud structure, and further reduce the data volume.

Voxel Encoding. After the above point cloud preprocessing, the voxel encoder in Uni-Hand encodes the dense 3D voxels into a sparser representation $X^{\text{vox}} \in \mathbb{R}^{N_{\text{vox}} \times f}$ through 3D convolutions. That is, each input point cloud corresponds to N_{vox} voxel patches with the same channel dimension f as HM latents. Notably, while these voxel patches share dimensional alignment with HM latents, we do not integrate them into HM latents. Instead, they are maintained as separate global contexts of 3D interaction environments for the denoising model in the following HMF diffusion. This stems from the fact that the unified global representation of aggregated point clouds has not been time-varying compared to sequential egocentric observations. Merging it into time-varying HM latents is not required.

3.3 Dual-Branch Diffusion Model

3.3.1 Hand-Head Motion Coordination

Our proposed dual-brach diffusion model is aimed at capturing the synergy between hand movements and headset camera egomotion, and concurrently predicting future HM latents and EM latents. The hand-head motion coordination within the future interaction process is reflected in three aspects: (1) Hand movements often follow head motion, as the head's prior motion provides key visual cues for trajectory planning (Fig. 5(a)), (2) head movements may follow hand actions, as subconscious and faster hand motions can lead to head responses (Fig. 5(b)), and (3) humans

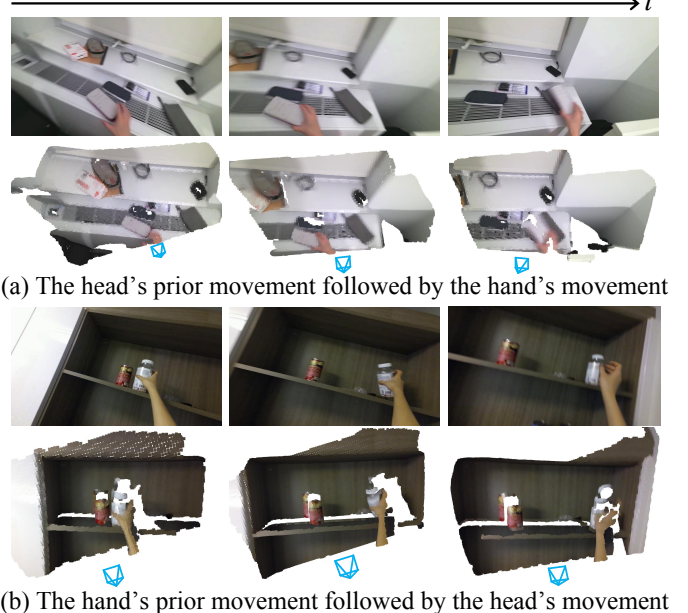


Fig. 5: Examples of head movement (corresponding to camera egomotion) and hand movement entangled during the hand-object interaction process in egocentric views in the EgoPAT3D dataset [66]. Here we present the RGB images and point clouds, as well as camera poses to clarify the hand-head motion trend.

keep hand movements within egocentric views to ensure accurate target contact (Fig. 5(a) and Fig. 5(b)). We argue that predicting hand motion agnostic to future head motion does not align with real human behavior planning. Instead, explicitly decoupling the entangled hand-head movements helps prediction models to better understand synergy motion patterns and potential intentions of interaction. In light of this, we propose the dual-branch diffusion model, encompassing the EMF diffusion and HMF diffusion to predict future EM latents (headset camera egomotion) and HM latents (hand motion) concurrently.

3.3.2 EMF Diffusion

The EMF diffusion is developed to denoise future EM latents, thus obtaining the future head motion trend for the following hand motion forecasting. As shown in Fig. 2(b), the EMF diffusion leverages Mamba [21] as the denoising model to convert the noisy future EM latents $F_{\text{noise}}^{\text{em}}$ to $\hat{F}_{\text{f}}^{\text{em}} \in \mathbb{R}^{N_{\text{f}} \times f}$ conditioned on the past EM latents F_{p}^{em} . The predicted $\hat{F}_{\text{f}}^{\text{em}}$ implicitly represents future head motion trend during the interaction process. Since the head movement patterns are much simpler than those of moving hands, we propose using the vanilla Mamba blocks for efficient denoising. Besides, we omit the process of decoding the future EM latents into specific homography matrices. This eliminates the ambiguity inherent in selecting supervision signals for alternative homography parameterizations [67].

3.3.3 HMF Diffusion

With the predicted camera egomotion trend, the HMF diffusion aims to forecast future HM latents, which will be transformed into the explicit future hand trajectories and interaction states by the devised decoders. As shown in

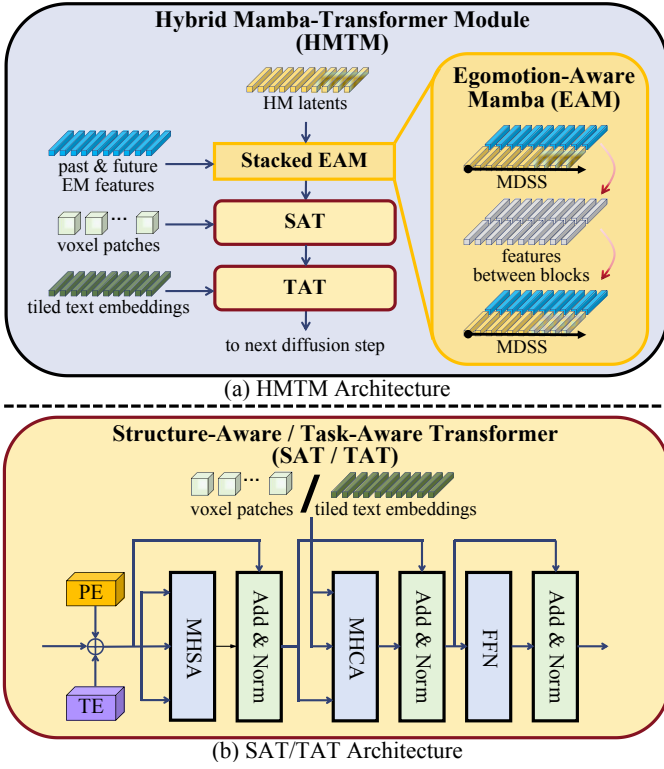


Fig. 6: Architecture of the hybrid Mamba-Transformer module. It denoises HM latents with stacked EAM, SAT, and TAT blocks.

Fig. 2(b), the HMF diffusion receives past HM latents F_p^{hm} to predict future counterparts \hat{F}_f^{hm} , conditioned on F_p^{em} and \hat{F}_f^{em} predicted by the EMF diffusion. Here we propose a novel hybrid Mamba-Transformer module (HMTM) as the denoising model. As showcased in Fig. 6(a), HMTM comprises three key components: (1) stacked egomotion-aware Mamba (EAM) blocks adapted from MADiff [16], which employ Motion-Driven Selective Scan (MDSS) to seamlessly incorporate egomotion homography features into Mamba's state transitions, (2) our newly designed structure-aware Transformer (SAT), which absorbs voxel patches as 3D global context by multi-head cross-attention, and (3) task-aware Transformer (TAT), where we inject text embeddings of task instructions into the HMF denoising process.

Stacked Egomotion-Aware Mamba (EAM). Concretely, we first concatenate F_p^{em} with the predicted \hat{F}_f^{em} to $\hat{F}_{pf}^{\text{em}} \in \mathbb{R}^{(N_p+N_f) \times f}$ along the time dimension, leading to the holistic feature sequence of headset camera egomotion in past and future time horizons. Similarly, we concatenate F_p^{hm} with the sampled noise $F_{\text{noise}}^{\text{hm}}$ to $F_{pf}^{\text{hm}} \in \mathbb{R}^{(N_p+N_f) \times f}$. Then we implement MDSS in EAM for each denoising step of the HMF diffusion, to denoise the future part of F_{pf}^{hm} conditioned on the holistic sequential EM latents \hat{F}_{pf}^{em} . Therefore, we integrate Mamba's powerful ability of temporal feature modeling, as well as head motion awareness into our framework. We refer more details of MDSS to the previous work [16].

Structure-Aware Transformer (SAT). The output of the stacked EMA blocks is further processed by the structure-aware Transformer in HMTM. SAT explicitly absorbs 3D global contexts of interaction environments for each denoising step of the HMF diffusion. As illustrated in Fig. 6(b), af-

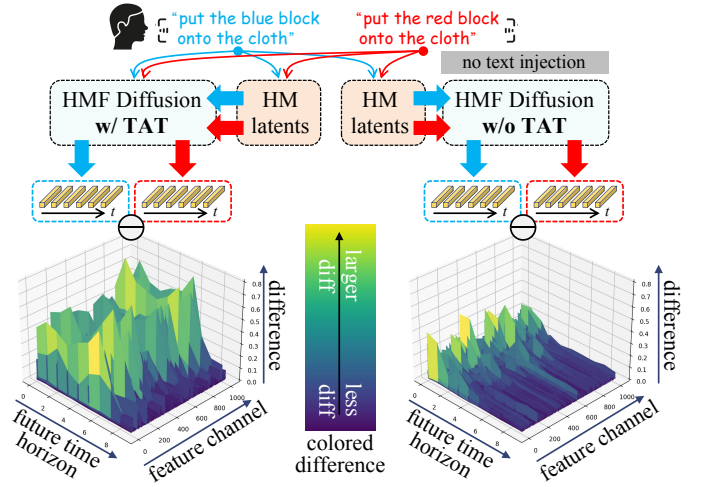


Fig. 7: Difference matrices of denoised future HM latents between two text instructions, “put the blue block onto the square cloth” and “put the red block onto the square cloth”. They are visualized as height fields. This illustration reflects the effectiveness of our devised TAT to enhance the awareness of specific tasks in hand feature prediction.

ter the standard positional/temporal encoding (PE/TE) [40], [15], we sequentially implement multi-head self-attention (MHSA) on HM latents F_{pf}^{hm} , and multi-head cross-attention (MHCA) between the output of MHSA and voxel patches X^{vox} . Specifically, for MHCA input, we use the HM latents from the preceding MHSA and Add&Norm as the query, and let the voxel patches X^{vox} be the key and value. Inspired by human perception of 3D spatial relationships with stereo vision, Uni-Hand incorporates voxel patches as environmental global context through MHCA in each denoising step. This enables more plausible hand motion forecasting thanks to the potential layout understanding and collision avoidance from 3D structure awareness.

Task-Aware Transformer (TAT). Following the devised SAT, the task-aware Transformer injects specific task information into hand motion forecasting. It facilitates the model's awareness of specific human intentions or downstream task instructions. As shown in Fig. 6(b), TAT has the same architecture as SAT. However, it performs multi-head cross-attention between the output of its MHSA and the tiled text embeddings X^{task} of the task instruction. We found that only merging the task-aware text embeddings into HM latents (introduced in Sec. 3.2.2) is not enough to facilitate generating future hand waypoints that comply with the input task instruction. The reason could be that the task specificity inherent in HM latents is continuously weakened as the network depth increases and progressive denoising operations are performed in the HMF diffusion. We thus need to continuously inject original task information by MHCA to enhance the model's task discrimination capability. Fig. 7 illustrates the different matrices of denoised future HM latents between two text instructions, “put the blue block onto the square cloth” and “put the red block onto the square cloth”. They are computed by $|\hat{F}_f^{\text{hm},\text{blue}} - \hat{F}_f^{\text{hm},\text{red}}|$ to present the feature difference from the two generally similar text instructions with different key targets (blue block vs. red block). As can be seen, after introducing the task-aware Transformer, besides only fusing

text embeddings into HM latents, the feature discrepancies between the predicted future HM latents are significantly pronounced. That is, TAT helps the prediction model to distinguish different interaction tasks for more reasonable hand motion forecasting. Its positive effect becomes more obvious in later timings, which will directly decide how well the predicted hand motion interacts with the target object. We will further ablate the task-aware text embedding injection in Sec. 4.6. Note that we deploy TAT in Uni-Hand only when the task being performed by human hands is known to us. The output latents of SAT will be directly fed to the next diffusion step in task-agnostic HMF.

After the last denoising diffusion step in the HMF diffusion, we obtain the denoised HM latents $\hat{F}_{\text{pf}}^{\text{hm}}$. As shown in Fig. 2(b), the future part $\hat{F}_{\text{f}}^{\text{hm}} \in \mathbb{R}^{N_f \times f}$ of $\hat{F}_{\text{pf}}^{\text{hm}}$ is ultimately decoded by the MLP-based hand trajectory decoder and interaction state decoder to future 2D/3D hand waypoints $\hat{\mathcal{H}}_{\text{f}} = \{\hat{H}_t\}_{t=1}^{N_f}$ and future interaction states $\hat{\mathcal{G}}_{\text{f}} = \{\hat{G}_t\}_{t=1}^{N_f}$. The denoised HM features, predicted waypoints and interaction states, can also be regarded as affordances for multiple downstream tasks, which will be validated in Sec. 4.5.

3.4 Training and Inference

3.4.1 Partial Noising and Denoising

We exploit partial noising/denoising proposed by Gong *et al.* [40] for the training and inference stages of both EMF diffusion and HMF diffusion. Specifically, we anchor the past latents F_{p}^{em} and F_{p}^{hm} in forward and reverse steps. In practice, although the EM latents and HM latents from the past time horizons are modified by noise corruption and denoising operations, they are manually overridden with their initial values (obtained via Multi-Modal Feature Extraction) after each diffusion step.

3.4.2 Loss Functions

We train Uni-Hand end-to-end, using six losses: (1) $\mathcal{L}_{\text{VLB}}^{\text{em}}$ for recovering future EM latents in the EMF diffusion, (2) $\mathcal{L}_{\text{VLB}}^{\text{hm}}$ for recovering future HM latents in the HMF diffusion, (3) trajectory displacement loss \mathcal{L}_{dis} , (4) trajectory angle loss $\mathcal{L}_{\text{angle}}$, (5) regularization term \mathcal{L}_{reg} , and (6) interaction state loss $\mathcal{L}_{\text{state}}$. We detail these losses as follows.

Losses for EMF Diffusion. To generate reasonable motion trends of the headset camera by the EMF diffusion, we set $\mathcal{L}_{\text{VLB}}^{\text{em}}$ for recovering future EM latents following the diffusion-related loss used by [15]:

$$\mathcal{L}_{\text{VLB}}^{\text{em}} = \sum_{s=2}^S \|\mathbf{z}_0^{\text{em}} - f_{\text{EMF}}(\mathbf{z}_s^{\text{em}}, s)\|^2 + \|F_{\text{f}}^{\text{em}} - \hat{F}_{\text{f}}^{\text{em}}\|^2, \quad (1)$$

where s is the index of each diffusion step, and S is the total diffusion steps. \mathbf{z}_s^{em} is the latent after the s -th denoising step. f_{EMF} denotes the function of the denoising model in the EMF diffusion. F_{f}^{em} is the GT future EM latents from the observations in future time horizons, and $\hat{F}_{\text{f}}^{\text{em}}$ is the counterparts finally predicted by the EMF diffusion as mentioned before.

Losses for HMF Diffusion. The diffusion-related loss $\mathcal{L}_{\text{VLB}}^{\text{hm}}$ supervising the predicted future HM latents in the HMF diffusion is similarly defined as:

$$\mathcal{L}_{\text{VLB}}^{\text{hm}} = \sum_{s=2}^S \|\mathbf{z}_0^{\text{hm}} - f_{\text{HMF}}(\mathbf{z}_s^{\text{hm}}, s)\|^2 + \|F_{\text{f}}^{\text{hm}} - \hat{F}_{\text{f}}^{\text{hm}}\|^2, \quad (2)$$

where \mathbf{z}_s^{hm} indicates the latent after the s -th denoising step. f_{HMF} represents the function of the denoising model in the HMF diffusion. F_{f}^{hm} is the GT future HM latents encoded from the observations in future time horizons. $\hat{F}_{\text{f}}^{\text{hm}}$ is the counterparts predicted by the HMF diffusion.

In addition, we utilize the trajectory displacement loss \mathcal{L}_{dis} and the trajectory angle loss $\mathcal{L}_{\text{angle}}$ to optimize the hand waypoints decoded by the hand trajectory decoder, which are expressed as:

$$\mathcal{L}_{\text{dis}} = \frac{1}{N_f} \sum_{t=1}^{N_f} D_{\text{dis}}(H_t, \hat{H}_t), \quad (3)$$

$$\mathcal{L}_{\text{angle}} = \frac{1}{N_f} \sum_{t=0}^{N_f-1} D_{\text{cos}}(H_{t+1} - H_t, \hat{H}_{t+1} - \hat{H}_t), \quad (4)$$

where $D_{\text{dis}}(\cdot)$ denotes the Euclidean distance between predicted hand waypoints and GT ones. \hat{H}_t is the output hand waypoints of the hand trajectory decoder, while H_t is its GT counterpart. $D_{\text{cos}}(\cdot)$ represents the cosine similarity between two input motion vectors.

Following the previous works [15], [16], we also introduce the regularization term \mathcal{L}_{reg} to penalize the difference between the pseudo trajectory predictions \tilde{H}_t and H_t as:

$$\mathcal{L}_{\text{reg}} = \frac{1}{N_f} \sum_{t=1}^{N_f} D_{\text{dis}}(H_t, \tilde{H}_t), \quad (5)$$

where \tilde{H}_t is obtained by directly feeding F_{f}^{hm} to the hand trajectory decoder rather than the predicted $\hat{F}_{\text{f}}^{\text{hm}}$. This regularization helps to improve training stability and optimization performance.

To optimize interaction state forecasting, we utilize the interaction state loss \mathcal{L}_{int} defined as:

$$\mathcal{L}_{\text{int}} = \text{CE}(\mathcal{G}_{\text{f}}, \hat{\mathcal{G}}_{\text{f}}), \quad (6)$$

where $\text{CE}(\cdot)$ is the binary cross-entropy loss function. $\hat{\mathcal{G}}_{\text{f}}$ is the predicted interaction states decoded by the interaction state decoder, and \mathcal{G}_{f} is its GT label. Through the supervision of the interaction state loss, the timings of hand-object contact will be predicted with probabilities closer to 1.

Total Loss Function. The total loss function to train our proposed Uni-Hand is the weighted sum of all the above losses, which is expressed as:

$$\mathcal{L}_{\text{total}} = \lambda_{\text{VLB}}^{\text{em}} \mathcal{L}_{\text{VLB}}^{\text{em}} + \lambda_{\text{VLB}}^{\text{hm}} \mathcal{L}_{\text{VLB}}^{\text{hm}} + \lambda_{\text{dis}} \mathcal{L}_{\text{dis}} + \lambda_{\text{angle}} \mathcal{L}_{\text{angle}} + \lambda_{\text{reg}} \mathcal{L}_{\text{reg}} + \lambda_{\text{int}} \mathcal{L}_{\text{int}}, \quad (7)$$

where $\lambda_{\text{VLB}}^{\text{em}}$, $\lambda_{\text{VLB}}^{\text{hm}}$, λ_{dis} , λ_{angle} , λ_{reg} , and λ_{int} are weights to balance the trade-off between these losses.

4 EXPERIMENTAL RESULTS

4.1 Benchmarks

We evaluate our proposed Uni-Hand and the existing baselines on four publicly available datasets including EgoPAT3D-DT [66], [14], H2O-PT [68], [14], HOT3D-Clips [69], and Epic-Kitchens-55 [70], and two self-recorded datasets including the Cup-Apple-Box-Hand (CABH) benchmark and Hand-ALOHA-Transfer (HAT) benchmark. In the HAT benchmark, we conduct human-robot transfer experiments on a real robot platform,

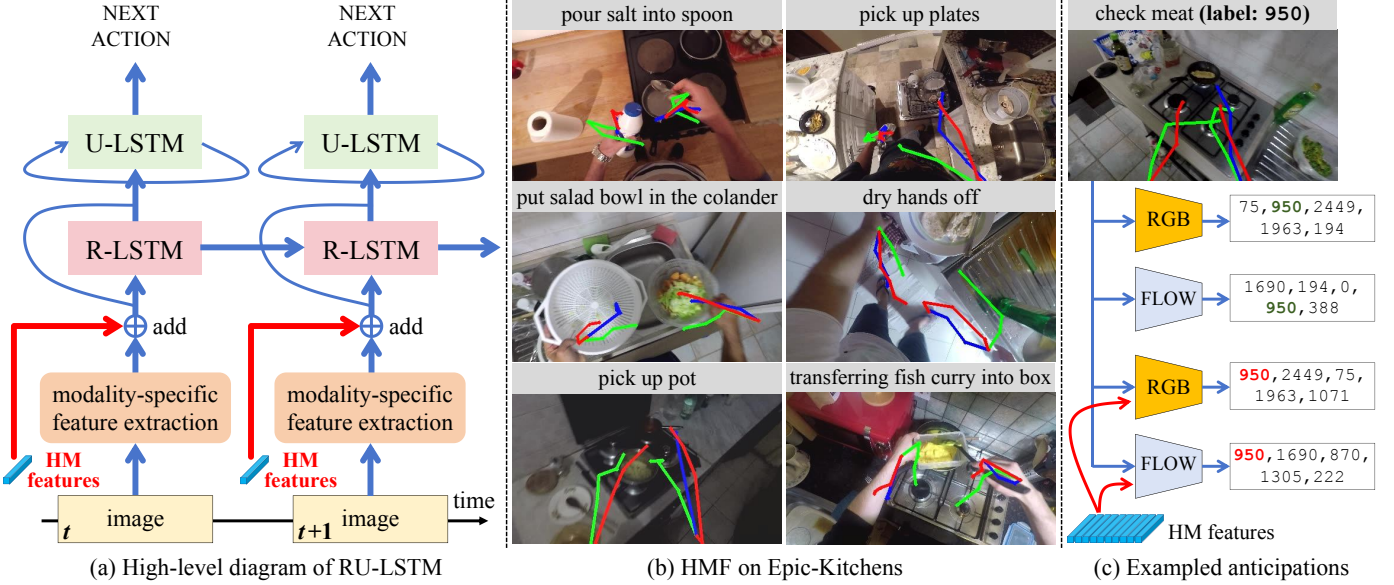


Fig. 8: Illustration of testing Uni-Hand in the downstream action anticipation task. In the egocentric images of (b) and (c), the red, green, and blue lines denote hand center waypoints predicted by Uni-Hand, OCT [13], and GT labels, respectively.

ALOHA [71], to present how Uni-Hand effectively supports manipulation tasks in real-world setups.

4.1.1 Public Datasets

We follow the setups of the prior works [14], [19] to organize EgoPAT3D-DT, H2O-PT, and HOT3D-Clips datasets. Please refer to Supp. Mat., Sec. A for more details. To further demonstrate how our Uni-Hand supports the downstream action anticipation, early action recognition, and action recognition tasks, we organize the Epic-Kitchens-55 dataset following the splits of OCT [13]. The evaluation paradigm for the downstream action anticipation task is illustrated in Fig. 8. As shown in Fig. 8(a), we select the widely-used and off-the-shelf action anticipation framework, RU-LSTM [54], to present the feature enhancement from our HMF method. Concretely, we first train Uni-Hand with annotated hand center waypoints in Epic-Kitchens-55, leading to a good HMF capability as depicted in Fig. 8(b). Afterwards, when implementing downstream action anticipation, we directly add the HM features (latents recovered by HMF diffusion of Uni-Hand) to the modality-specific features from the vanilla RU-LSTM. The combined features are further processed by the following rolling-unrolling operations through R-LSTM and U-LSTM. Then we optimize RU-LSTM for the action anticipation task, by minimizing the loss between the predicted action categories (linearly transformed from U-LSTM outputs) and the ground-truth labels. Note that we consider the modality-specific branches of RU-LSTM, i.e., the RGB branch and the flow branch, to demonstrate that our HMF method can enhance both RGB and flow features for higher anticipation accuracy. We do not use the object branch of RU-LSTM due to the mismatch in channel dimensions between HMF latents and object features. The feature enhancement operations for early action recognition and action recognition tasks are similar to action anticipation, while we only consider the ANTICIPATION period of RU-LSTM and discard its ENCODING period. Please refer more details about RU-LSTM structures to the original paper [54].

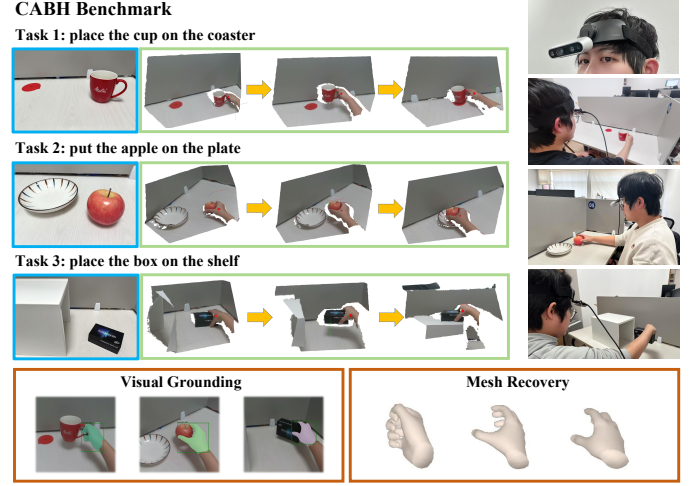


Fig. 9: Our self-collected CABH benchmark includes three hand-object interaction tasks to efficiently evaluate HMF methods.

4.1.2 Cup-Apple-Box-Hand Benchmark

To further demonstrate that our method has the potential to scale up with low-cost devices for data collection, we used headset RealSense D435i to collect 1200 egocentric videos for three real-world tasks, i.e., *place the cup on the coaster* (Task 1), *put the apple on the plate* (Task 2), and *place the box on the shelf* (Task 3), to build the CABH benchmark (see Fig. 9). For each task, 350 video clips are used for training with the other 50 clips for evaluation. Each clip has around 5 seconds, with the first 50% regarded as the past sequences and the latter 50% as the future ones. To validate that Uni-Hand can achieve plausible hand motion forecasting using only egocentric vision without expensive MoCap systems for GT annotations, we utilize the visual grounding model, Grounded SAM [72], and the hand mesh recovery approach, HaMeR [25], to label 2D hand centers and joints on videos. Their 3D positions can be further recovered with depth observations of the RGB-D camera.

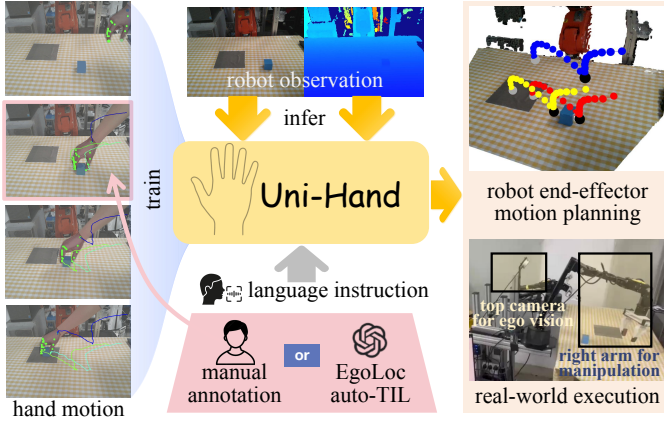


Fig. 10: Our scheme to deploy Uni-Hand to real-world robotic manipulation tasks.

To demonstrate that the choice of prediction canvas does not constrain the superiority of our proposed method, we directly predict future hand waypoints with each future frame as the canvas.

4.1.3 Hand-ALOHA-Transfer Benchmark

Task Definition. We also propose the Hand-ALOHA-Transfer benchmark by recording hand motion with the top camera mounted on ALOHA [71], as shown in Fig. 10. The top camera, RealSense LiDAR Camera L515, captures egocentric RGB images and point clouds (depth) for hand motion forecasting and end-effector action prediction. In the HAT benchmark, we introduce **five** manipulation tasks:

- **Push Task (♥):** push the block onto the cloth. 400 hand motion videos in total for training Uni-Hand. 10 trials to evaluate real-world performance.
- **Pick-and-Place Task (♦):** put the block onto the cloth. 400 hand motion videos in total for training Uni-Hand. 10 trials to evaluate real-world performance.
- **Harder Pick-and-Place Task (♣):** stack the blue block onto the red block. 400 hand motion videos in total for training Uni-Hand. 10 trials to evaluate real-world performance.
- **Language-Conditioned Pick-and-Place Task (♠):** put the {blue, red} block onto the cloth. 800 hand motion videos in total for training Uni-Hand, 400 videos per category (blue, red). 10 trials to evaluate real-world performance, 5 trials per category.
- **Long-Horizon Pick-and-Place Task (★):** put the block, the toy, and the banana onto the plate. 800 hand motion videos in total for training Uni-Hand. 10 trials to evaluate real-world performance.

These multiple manipulation tasks are used to evaluate both HMF performance and human-robot policy transfer ability.

Deployment Scheme. As illustrated in Fig. 10, we train Uni-Hand with recorded hand motion data, enabling it to generate complete executable actions for the robot end-effector in a look-then-move manner. Concretely, the predicted 3D trajectories are used for tracking, and the predicted interaction states help the robot to decide when to open and close its gripper. The GT 3D hand waypoints are captured by HaMeR [25]. To label the GT interaction states, we introduce two approaches: (1) manual annotation, and (2) automated temporal interaction localization (auto-TIL) using EgoLoc [73]. Note that this deployment scheme

is slightly different from the conventional HMF scheme, which always requires sequential past frames to forecast future motion. In both the training and inference stages with the HAT benchmark, only the first observation frame (i.e., $N_p = 1$, agnostic to hands) is used as the egocentric visual inputs. The prediction model directly predicts the global motion with complete waypoints and interaction states, instead of step-by-step reasoning conditioned on iterative observations and states. This is because the robot manipulates autonomously without visual access to human hands, depending entirely on environmental observations. We should not encode observations involving human hands in the training stage. Our HAT benchmark thus evaluates the HMF methods' ability to generate the holistic trajectory and interaction states from scratch without the constraints of observed motion. Besides, our work attends to forecasting reasonable hand waypoints and interaction states, rather than fine-grained 3D hand-object interaction (HOI) analysis. Therefore, for all the robotic manipulation tasks in this benchmark, we curate the mapping from human hand grasp poses to robot grasp poses, which is detailed in Supp. Mat., Sec. C.

4.2 Uni-Hand Configurations

For vision-language features from RGB images and universal text prompt shown in Fig. 3, we extract the outputs of the deepest cross-modality multi-head attention module (X-MHA) in GLIP [63], which are further processed by the channel adapter proposed by [16]. Besides, in Fig. 3, the channel dimension of all the features before concatenation is set as 1024, and the counterpart of the target indicators is determined by the number of prediction targets (e.g., 5 if predicting five hand joints). To generate 3D global context shown in Fig. 4, we convert input point clouds into voxel grids of dimensions $20 \times 20 \times 20$ with a resolution of 0.05 m. Each voxel patch has a size of 27×1024 . For both EMF diffusion and HMF diffusion, we set the channel dimension of the latent features to 1024. The total number of diffusion steps is set to 1000, while the EMF diffusion takes only one step to predict EM latents for high efficiency, and the HMF diffusion takes 100 steps to predict future HM latents. We adaptively adjust the input and output dimension of the MLPs for encoding and decoding hand trajectories according to the predictive space (2D/3D). We only activate the interaction state decoder for our HAT benchmark since only this benchmark has GT hand-object contact/separation state annotations. Notably, for hand-ALOHA motion transfer, the camera homography is an identity matrix since the robot base is fixed in our HAT benchmark. Besides, we empirically found that the HMF diffusion can generate more stable trajectories for the robot end-effector when increasing the denoising steps to 1000. There is a trade-off between inference efficiency and planning accuracy. The hybrid pattern of Mamba and Transformer in our devised hybrid Mamba-Transformer module is designed according to the ablation study in Supp. Mat., Sec. D. We train Uni-Hand using AdamW optimizer [74] with a learning rate of 5e-5 for 1K epochs on EgoPAT3D-DT, H2O-PT, and our self-recorded benchmarks, and with a learning rate of 5e-6 for 2K epochs on the HOT3D-Clips dataset. We will provide more Uni-Hand setups in our open-source repository.

TABLE 1: Comparison of performance on 3D hand trajectory prediction on the publicly available datasets. Best and secondary results are viewed in **bold black** and **blue** colors respectively.

Approach	EgoPAT3D-DT (seen)		EgoPAT3D-DT (unseen)		H2O-PT		HOT3D-Clips	
	ADE \downarrow	FDE \downarrow	ADE \downarrow	FDE \downarrow	ADE \downarrow	FDE \downarrow	ADE \downarrow	FDE \downarrow
CVH [15]	1.100	1.278	0.952	1.018	0.146	0.148	1.273	1.358
OCT* [13]	0.370	0.524	0.309	0.397	0.103	0.126	0.188	0.215
USST* [14]	0.183	0.341	0.120	0.185	0.031	0.052	0.123	0.157
S-Mamba [75]	0.185	0.355	0.138	0.207	0.038	0.074	0.117	0.132
Diff-IP3D [15]	0.199	0.377	0.156	0.229	0.049	0.081	0.147	0.164
MADiff3D [16]	0.183	0.363	0.139	0.224	0.032	0.059	0.120	0.147
Uni-Hand (ours)	0.170	0.336	0.118	0.189	0.030	0.050	0.104	0.131

* The baselines are re-evaluated according to the erratum: <https://github.com/oppo-us-research/USST/commit/beebdb963a702b08de3a4cf8d1ac9924b544abc4>.

TABLE 2: Comparison of performance on 2D hand trajectory prediction on the publicly available datasets. Best and secondary results are viewed in **bold black** and **blue** colors respectively.

Approach	EgoPAT3D-DT (seen)		EgoPAT3D-DT (unseen)		H2O-PT		HOT3D-Clips	
	ADE \downarrow	FDE \downarrow	ADE \downarrow	FDE \downarrow	ADE \downarrow	FDE \downarrow	ADE \downarrow	FDE \downarrow
CVH [15]	0.180	0.230	0.188	0.221	0.206	0.208	0.437	0.444
OCT* [13]	0.108	0.122	0.091	0.147	0.387	0.381	0.190	0.240
USST* [14]	0.082	0.118	0.060	0.087	0.040	0.068	0.133	0.172
S-Mamba [75]	0.084	0.141	0.071	0.118	0.051	0.094	0.130	0.160
Diff-IP2D [15]	0.080	0.130	0.066	0.087	0.042	0.074	0.169	0.208
MADiff [16]	0.065	0.105	0.054	0.086	0.039	0.068	0.124	0.160
Uni-Hand (ours)	0.064	0.109	0.052	0.087	0.036	0.065	0.118	0.156

TABLE 3: Comparison of performance on hand trajectory prediction on our CABH in 3D and 2D spaces. Best and secondary results are viewed in **bold black** and **blue** colors.

Approach	Task 1		Task 2		Task 3		3D metrics
	ADE \downarrow	FDE \downarrow	ADE \downarrow	FDE \downarrow	ADE \downarrow	FDE \downarrow	
USST [14]	0.102	0.125	0.109	0.128	0.103	0.130	
Diff-IP3D [15]	0.053	0.057	0.055	0.078	0.064	0.080	
S-Mamba [75]	0.045	0.055	0.050	0.072	0.058	0.061	
Uni-Hand (ours)	0.041	0.052	0.044	0.061	0.047	0.053	
2D metrics							
USST [14]	0.115	0.155	0.127	0.168	0.124	0.161	
Diff-IP2D [15]	0.084	0.100	0.094	0.117	0.109	0.126	
S-Mamba [75]	0.080	0.102	0.081	0.107	0.102	0.108	
Uni-Hand (ours)	0.066	0.086	0.077	0.099	0.094	0.095	

4.3 Evaluation on Multi-Dimensional Hand Trajectory Prediction

We first validate our claim that the proposed Uni-Hand predicts plausible hand center waypoints in both 2D and 3D dimensions. Predicting hand centers constitutes the most fundamental capability required by the HMF method. The evaluation metrics including averaged displacement error (ADE) and final displacement error (FDE) are reported following the previous works [14], [15], [22]. The prediction canvas [15] is selected as the first frame of each video clip. That is, all the 3D waypoints are expressed relative to the first camera coordinate, and all the 2D waypoints are transformed to the first image plane. The evaluation in the 3D space follows the absolute scale in meters. For the evaluation in 2D space, we normalize the predicted waypoint pixel coordinates by the image size. We separately forecast left- and right-hand motion. We compare our Uni-Hand with the existing baselines including Constant Velocity Hand (CVH) [15], OCT [13], USST [14], S-Mamba [75], Diff-IP2D [15], and MADiff [16]. We modify S-Mamba [75] originally designed for general time series forecasting into

our diffusion-based paradigm to predict HM tokens. We additionally replace the 2D input and output, and the corresponding encoders and decoders with 3D counterparts in Diff-IP2D [15] and MADiff [75] since they were originally developed for 2D forecasting tasks, obtaining the baselines Diff-IP3D and MADiff3D.

Here we present the center prediction performance of our proposed Uni-Hand and the baselines on the publicly available datasets and our CABH benchmark. As Tab. 1, Tab. 2, and Tab. 3 show, Uni-Hand produces the lowest prediction errors on most metrics compared to the SOTA baselines. Although some baselines show competitive performance in 2D and 3D respectively, they show specialized and lack consistent superiority across both spaces due to a lack of multi-modal fusion. In contrast, our universal framework accommodates both 3D structure information and 2D camera egomotion, achieving consistently comparable performance in both 2D and 3D spaces. Fig. 11 and Fig. 12 visualize the predicted hand center waypoints, where Uni-Hand’s predictions have better stability and directionality in multiple dimensions. This suggests that Uni-Hand better captures hand motion patterns and potential human intentions during interaction by harmonizing multi-modal information. Moreover, HOT3D-Clips has small data volumes to supervise prediction models, where our Uni-Hand consistently outperforms the other baselines. This implies that our method better accommodates situations with limited training data.

4.4 Evaluation on Multi-Target Hand Trajectory Prediction

In this experiment, we validate the capability of our Uni-Hand to forecast plausible future waypoints of multiple hand joints rather than centers. We do not involve EgoPAT3D-DT here due to a lack of joint annotations. For the H2O-PT and HOT3D-Clips datasets which have labeled

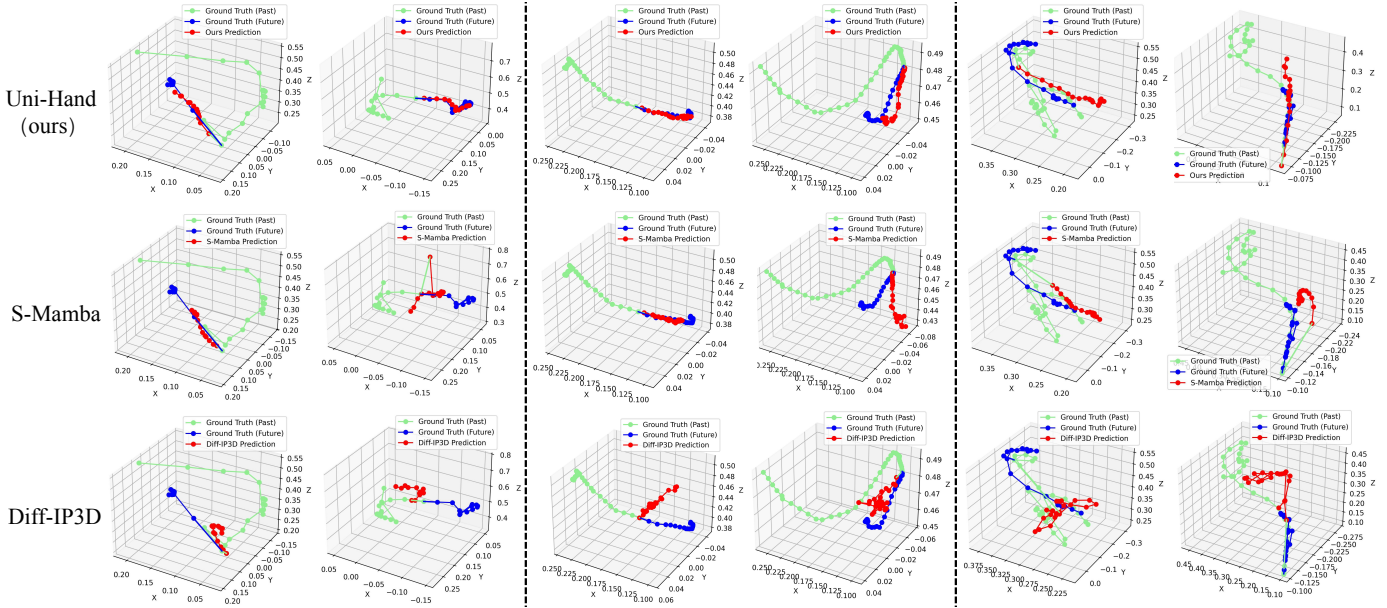


Fig. 11: Visualization of predicted hand trajectories in the 3D space (left: EgoPAT3D-DT; middle: H2O-PT; right: HOT3D-Clips). We show the holistic sequence including observed past hand waypoints (green), ground-truth future ones (blue), and predicted future counterparts (red) by our Uni-Hand and two SOTA baselines.

TABLE 4: Comparison of performance on multi-joint waypoint prediction in 3D space on the H2O-PT, HOT3D-Clips, and CABH-E. Best and secondary results are viewed in **bold black** and **blue** colors respectively.

Approach	H2O-PT		HOT3D-Clips		CABH-E	
	ADE \downarrow	FDE \downarrow	ADE \downarrow	FDE \downarrow	ADE \downarrow	FDE \downarrow
USST* [14]	0.102	0.123	0.162	0.180	0.105	0.122
Diff-IP3D [15]	0.152	0.160	0.200	0.204	0.093	0.110
S-Mamba [75]	0.046	0.087	0.200	0.229	0.099	0.130
Uni-Hand w/o X^{tar}	0.038	0.076	0.121	0.151	0.047	0.056
Uni-Hand (ours)	0.036	0.066	0.118	0.148	0.038	0.046

GT 3D joint positions, we predict trajectories of five joints: one on the wrist and two each on the thumb and index finger (see Supp. Mat., Sec. B). These prediction targets are selected according to the recent work [49] considering potential downstream tasks. Moreover, we provide a data extension of our CABH benchmark (CABH-E) compared to our preliminary version [19]. As shown in the first row of Fig. 13, we record “place the apple into the square area from multiple directions” to demonstrate that our Uni-Hand captures multimodal behavior [41] without generating jittery actions from multiple directions. For CABH-E, we also generate 3D GT positions by HaMeR with depth observations, and forecast trajectories of three joints, which are on the wrist, the thumb tip, and the middle fingertip (see Fig. 13). This target selection follows the setups from CoM [76], which emphasizes using the middle fingertips instead of the index ones. We thus showcase the performance of our proposed method on forecasting joint waypoints with different target combinations. The final displacement errors are averaged among the target joints. Note that the SOTA baselines in this experiment are implemented separately on different joints since they do not support multi-target prediction originally.

As showcased in Tab. 4, our proposed Uni-hand consistently outperforms the baselines on the three datasets. Especially for the CABH-E, Uni-hand reduces the ADE

and FDE of the second-best baseline by 0.055 and 0.064, respectively. We also visualize the predicted joints’ positions projected to the last frame of each input video clip in Fig. 13. Uni-Hand generally generates plausible joint waypoints extending in correct directions, with the final positions all successfully meeting the requirement of placing the apple in the target area. The above experimental results demonstrate that our universal framework achieves good multi-target hand forecasting, extending the scope of the existing hand trajectory prediction that only attends to hand centers.

Tab. 4 also ablates the contribution of our devised target indicators. The baseline Uni-Hand w/o X^{tar} separately forecasts different joints without using target indicators. The results indicate that although Uni-Hand w/o X^{tar} has outperformed the other SOTA baselines, Uni-Hand can better identify which joint it currently attends to, and predicts more accurate joint waypoints. Therefore, the target indicators are demonstrated as key components in our universal HMF framework to achieve multi-target forecasting.

4.5 Evaluation on Downstream Tasks

In this section, we evaluate the claim that our approach enables multi-task affordances for downstream applications, including human-robot manipulation policy transfer, action anticipation, early action recognition, and action recognition.

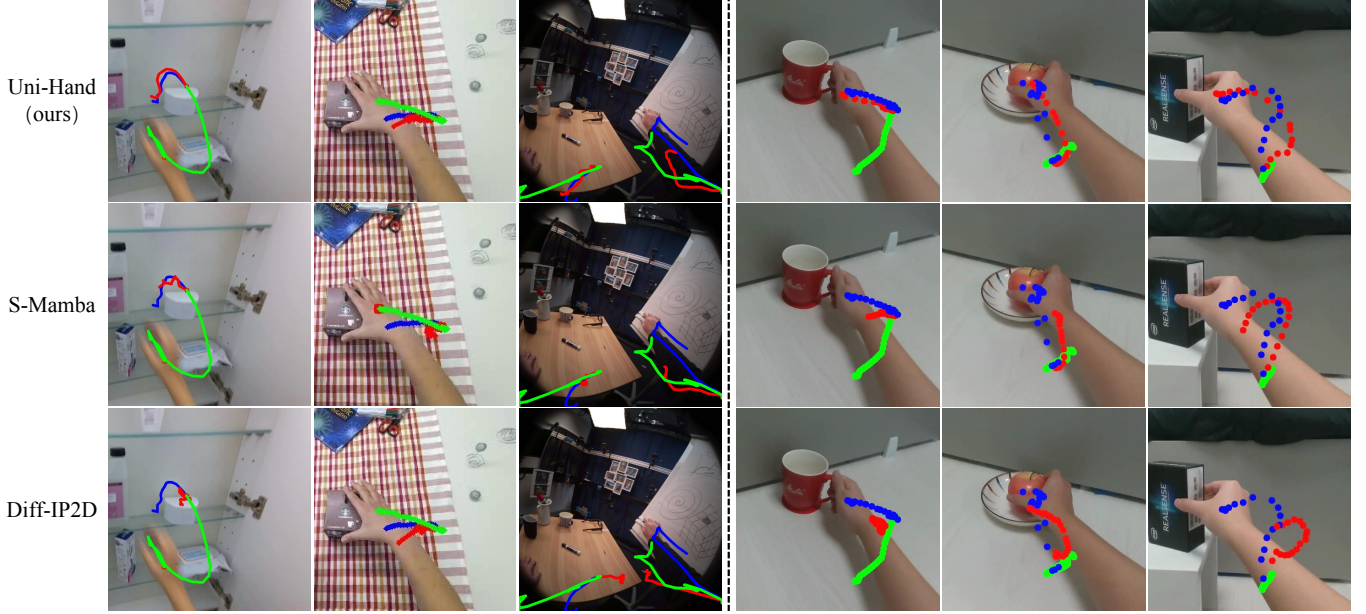


Fig. 12: Visualization of 2D hand center forecasting (left: EgoPAT3D-DT, H2O-PT, and HOT3D-Clips; right: CABH). We show the holistic sequence including observed past joint waypoints (green), ground-truth future ones (blue), and predicted future counterparts (red) by our Uni-Hand and two SOTA baselines. Here we showcase the predictions on the first frame of each input video clip for EgoPAT3D-DT, H2O-PT, and HOT3D-Clips, while presenting the last frame for our CABH.

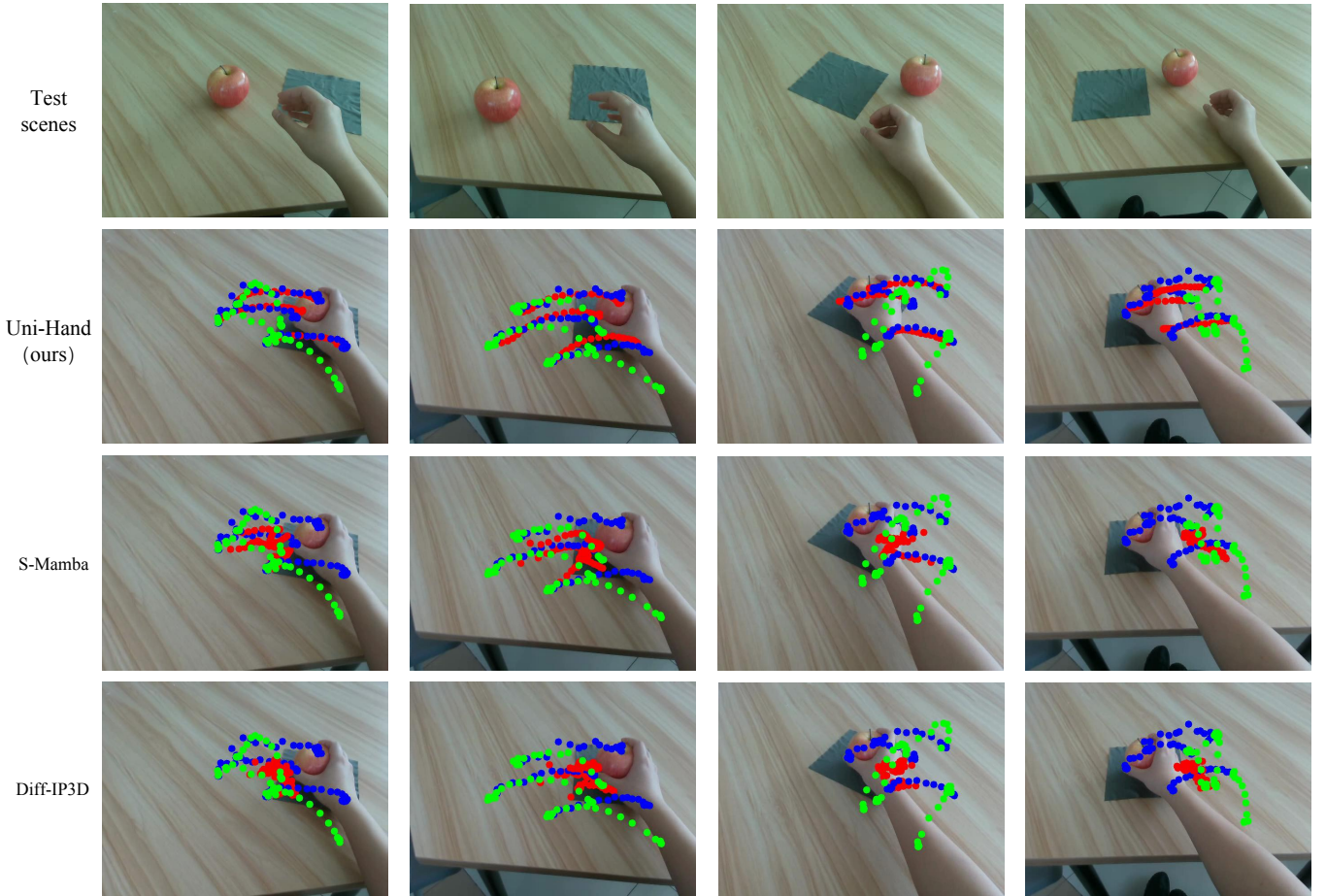


Fig. 13: Visualization of multi-target prediction on our CABH-E. We show the holistic sequence including observed past joint waypoints (green), ground-truth future ones (blue), and predicted future counterparts (red) by our Uni-Hand and two SOTA baselines. Here we showcase the predictions on the last frame of each input video clip.

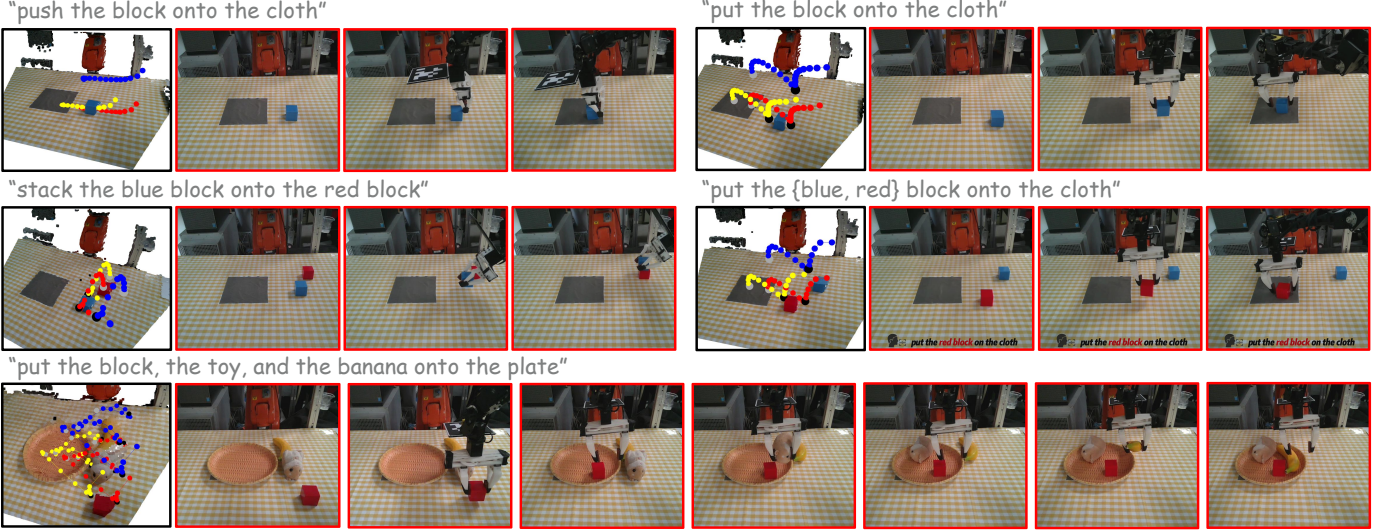


Fig. 14: Real-world test on ALOHA. For each manipulation task, we illustrate the trajectories generated from scratch by Uni-Hand and how the gripper follows the action planning. The blue dots denote the predicted hand wrist positions, which spawn the yellow and red dots corresponding to the index fingertip and the thumb tip. The black and grey dots denote the pick and place timings of the gripper, respectively.

4.5.1 Human-Robot Manipulation Policy Transfer

This experiment is conducted on our proposed Hand-ALOHA-Transfer benchmark to validate Uni-Hand’s ability to facilitate multiple downstream robotic manipulation tasks. The five tasks and prediction configurations in this benchmark have been detailed in Sec. 4.1.3. We activate the task-aware Transformer and inject the text embeddings of task instructions into it to enhance the model’s adherence to specific task setups. Here the GT interaction states are labeled manually by default. More experimental details and results with EgoLoc annotations will be introduced in Supp. Mat., Sec. E. Tab. 5 first shows the ADE and FDE metrics of Uni-Hand and the SOTA baseline S-Mamba in 3D on the validation sets of the real-world scenes. Uni-Hand generates end-effector trajectories that align better with human motion patterns. We also observed lower prediction errors around hand-object contact timings (see Supp. Mat., Sec. G), which suggests that hand movements hold lower uncertainties at these timings, leading to more stable supervision signals to optimize Uni-Hand. This also facilitates plausible action planning despite relatively higher errors at other timings (e.g., the initial stage). Besides, we also present the Mean Absolute Error (MAE) of the contact-separation/separation-contact transition timings within the predicted interaction states on these tasks. Since the baseline [75] is proposed without the ability for interaction state prediction, we do not report its MAE and directly use GT labels as its pseudo predictions for the following real-world execution. Tab. 5 shows that Uni-Hand predicts accurate hand-object contact/separation states for reasonable action planning in the following robot execution. Then, we directly transfer the prediction models to the real-world deployment, and let the end-effector follow the generated trajectories and grasp actions.

As showcased in Tab. 5, for 10 test trials of each designated manipulation task, our proposed Uni-Hand exhibits significant superiority with higher success rates than the

baseline S-Mamba. The baseline is infeasible with 0% SR for the harder pick-and-place, language-conditioned pick-and-place, and long-horizon pick-and-place tasks. Fig. 14 shows how the end-effector accurately follows Uni-Hand’s hand motion forecasting results for these tasks. This demonstrates that hand motion forecasting implemented by Uni-Hand provides the required motion knowledge for practical deployments on a real robot platform. It benefits policy learning for atomic skills such as push, pick, and place, and also holds promise for completing complex language-conditioned and long-horizon robotic tasks.

4.5.2 Action Anticipation

We have showcased in Fig. 8(b) that our Uni-Hand can predict good hand waypoints after being optimized on Epic-Kitchens. This indicates that Uni-Hand can generate reasonable hand motion features (HM features) related to specific future human activities. Therefore, we explore whether the future HM features can enhance the downstream action anticipation, a task that predicts which category of action will happen. As shown in Fig. 15, after we add the HM features recovered by our HMF diffusion to the vanilla modality-specific features in the RGB and flow branches of RU-LSTM, the Top-5 verb/noun/action accuracy increases at most anticipation times τ_a . Fig. 8(c) also presents an example of Top-5 action categories predicted by RU-LSTM before and after adding HM features. As can be seen, the feature enhancement by our HMF method facilitates a higher probability for the correct action category. These results highlight that the hand motion features predicted by Uni-Hand can be effective affordances encompassing future activity information for the downstream action anticipation.

4.5.3 Early Action Recognition and Action Recognition

Different from action anticipation, the downstream early action recognition and action recognition tasks focus on reasoning human activity categories according to partial

TABLE 5: Performance comparison on our proposed HAT benchmark. We present the errors of hand trajectory prediction and interaction state prediction on the validation set (20 out of the training samples), as well as the success rates (SR) of 10 test trials for each manipulation task.

Tasks	S-Mamba [75]				Uni-Hand (ours)			
	ADE \downarrow	FDE \downarrow	MAE \downarrow	SR \uparrow	ADE \downarrow	FDE \downarrow	MAE \downarrow	SR \uparrow
♥	0.038	0.049	-	40%	0.022	0.018	1.3	100%
♦	0.053	0.051	-	20%	0.035	0.012	1.9	90%
♣	0.061	0.040	-	0%	0.040	0.016	0.8	80%
♠	0.075	0.076	-	0%	0.054	0.028	1.8	80%
★	0.100	0.109	-	0%	0.059	0.071	1.9	20%

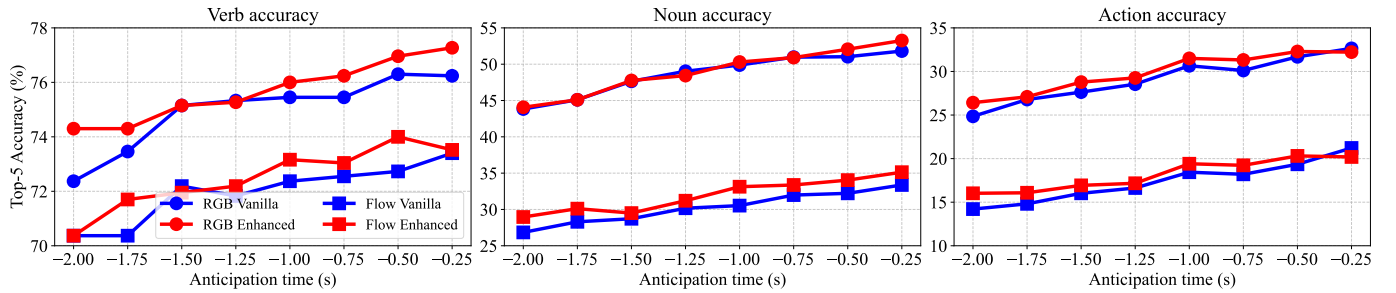


Fig. 15: Performance comparison between RU-LSTM branches enhanced by our Uni-Hand’s HM features and the vanilla model on the downstream action anticipation task. We follow the evaluation metrics of the prior work [54].

TABLE 6: Top-5 action accuracy (%) of RU-LSTM branches on the downstream early action recognition and action recognition tasks. We present the performance at the observation rates 12.5% \sim 87.5% for early action recognition, and 100% for action recognition following [54]. Best results are viewed in **bold black**.

Approach	Early action recognition						
	12.5%	25.0%	37.5%	50.0%	62.5%	75.0%	87.5%
RGB (vanilla)	36.40	38.21	39.18	40.45	41.29	41.90	41.66
RGB (enhanced)	36.22	37.85	39.42	39.78	41.60	42.26	42.32
Flow (vanilla)	19.77	24.67	27.63	28.30	29.99	30.35	30.71
Flow (enhanced)	19.83	24.43	26.90	28.54	30.29	31.02	31.74
Approach	Action recognition (100%)						
	Centers	Multiple joints					
RGB (vanilla)	41.78						
RGB (enhanced)	42.74						
Flow (vanilla)	30.96						
Flow (enhanced)	31.74						

or complete observations. Following RU-LSTM [54], we simply discard its ENCODING period and only attend to the observations in the ANTICIPATION period. As noted in Tab. 6, after adding HM features from Uni-Hand, the recognition accuracy of RGB and flow branches in RU-LSTM increases at most observation rates. Note that we additionally train a Uni-Hand model to achieve multi-joint motion forecasting (the wrist, the thumb tip, and the index fingertip), and enhance RU-LSTM by adding these new HM features. For action recognition with the observation rate of 100%, HM features encompassing multi-joint motion information yield additional performance improvements. This further validates the advantages of multi-target predictions by our Uni-Hand. However, compared to the results of action anticipation in Fig. 15, the feature enhancement from Uni-Hand exhibits an overall weaker influence on these two downstream tasks. This suggests that the positive effect of predicted HM features diminishes when partial action observations are available. Nevertheless, Uni-Hand

TABLE 7: Ablation study on camera egomotion. SE(3) as egomotion represents the baseline replacing the input camera homography with 6-DOF poses. Uni-Hand w/o EMF represents the baseline without the EMF diffusion. Best results are viewed in **bold black**.

Approach	EgoPAT3D-DT (seen)		EgoPAT3D-DT (unseen)		H2O-PT	
	ADE \downarrow	FDE \downarrow	ADE \downarrow	FDE \downarrow	ADE \downarrow	FDE \downarrow
SE(3)	0.257	0.446	0.217	0.308	0.032	0.063
w/o EMF	0.186	0.363	0.137	0.231	0.031	0.053
Uni-Hand	0.170	0.336	0.118	0.189	0.030	0.050

still affords informative HM features for downstream action recognition thanks to a deeper understanding of hand motion patterns.

4.6 Ablation Studies

In this section, we experimentally demonstrate the positive effectiveness of different components tailored for Uni-Hand. We have ablated our devised target indicators for multi-target motion forecasting in Sec. 4.4. Here we conduct ablations on hand center forecasting in 3D. Please refer to Supp. Mat., Sec. D-F for more ablation experiments.

Camera Egomotion Forecasting. We first ablate the headset camera egomotion forecasting on EgoPAT3D-DT and H2O-PT. Concretely, we conduct a baseline by removing the EM Diffusion, and regarding the last past camera homography as the constant egomotion in future time horizons. We present the hand center forecasting performance in 3D space in Tab. 7. As can be noted, forecasting future headset camera egomotion improves the accuracy of hand waypoint forecasting. This demonstrates that our dual-branch diffusion model of Uni-Hand captures the synergy between head motion and hand motion for a better understanding of the future interaction process. Notably, the reduction in ADE and FDE is more significant on EgoPAT3D-DT compared to H2O-PT. This discrepancy may arise from the richer diversity of intense head motions in EgoPAT3D-DT, which offers stronger supervision on egomotion forecasting.

TABLE 8: Ablation study on multimodal inputs. Best results are viewed in **bold black**.

Input modalities	Seen	Unseen
waypoint image text point cloud	ADE ↓ FDE ↓	ADE ↓ FDE ↓
✓	0.178 0.356	0.124 0.205
✓ ✓	0.173 0.350	0.122 0.201
✓ ✓ ✓	0.171 0.347	0.122 0.200
✓ ✓ ✓ ✓	0.170 0.336	0.118 0.189

TABLE 9: Ablation study on text embedding injection. Best results are viewed in **bold black**.

Approach	ADE ↓	FDE ↓	MAE ↓	SR ↑
Uni-Hand w/o TAT	0.057	0.034	2.0	40%
Uni-Hand	0.054	0.028	1.8	80%

Camera Egomotion Representation. Despite the ablation studies on homography as camera egomotion provided by the previous works [15], [16], we additionally present the 3D hand center forecasting performance when we regard SE(3), i.e., 6-DOF poses from visual odometry, as camera egomotion in our framework instead of homography. As showcased in Tab. 7, replacing the vanilla egomotion homography with SE(3) leads to a significant degradation in HMF performance. This suggests that the homography-based representation is better suited for modeling egomotion in this context. It also aligns with the fact that observed hands are constrained to the 2D image plane, and homography matrices more effectively capture the camera egomotion variations coupled with hand motions.

Multi-Modal Inputs. We further ablate the combinations of multiple input modalities of Uni-Hand. We incrementally add past hand waypoints, RGB images, the universal text prompt, and point clouds in model inputs. The experimental results of 3D hand center forecasting on the EgoPAT3D-DT dataset shown in Tab. 8 indicate that our proposed framework well harmonizes multi-modal information to achieve strong forecasting performance. The incorporation of both the universal text prompt and point cloud data effectively bridges modality gaps in existing literature.

Text Embedding Injection. We have illustrated in Fig. 7 that our proposed text embedding injection in the hybrid Mamba-Transformer module facilitates the HM features denoised for task-aware hand motion forecasting. Here we further present the quantitative results on the validation and test sets of the task “put the {blue, red} block onto the cloth” of our HAT benchmark. We conduct the baseline, labeled Uni-Hand w/o TAT, by removing the task-aware Transformer in the denoising model. Tab. 9 indicates that the introduction of our devised text embedding injection with TAT reduces prediction errors, while also improving success rates significantly.

5 CONCLUSION

We have developed a universal framework namely Uni-Hand to achieve multi-dimensional and multi-target hand motion forecasting in egocentric views. Uni-Hand absorbs multi-modal data and predicts plausible hand trajectories in both 2D and 3D spaces, considering hand-head motion synergy. It attends to the future motion of hand centers and any joints, as well as hand-object interaction states. Extensive

experiments on public datasets and our newly proposed benchmarks have demonstrated that our universal framework outperforms the existing SOTA baselines in hand motion forecasting across 2D/3D spaces and multiple targets, and facilitates multi-task affordances for downstream applications, including robotic manipulation, action anticipation, early action recognition, and action recognition.

Insights and Limitations: Thanks to the low-cost and highly efficient nature of human video acquisition, our proposed framework can be efficiently optimized and may act as a foundation model for visual imitation learning. It generates reasonable action planning for robot manipulation in a look-then-move manner, and may be fine-tuned by robot data for further improvement. We also hope that our exploration of multi-modal harmonization, hand-head prediction decoupling, and task-aware text embedding injection could inspire future works on egocentric human-object interaction. Despite the encouraging results, our work still has the following limitations. Firstly, the final predicted hand positions are not represented in mesh/topological format. Although this improves training/inference efficiency while reducing non-essential joints’ interference, we will extend it to more thorough 3D HOI mesh recovery in each video clip. Additionally, we will generalize the proposed method to robots’ dexterous bimanual manipulation scenarios with movable top cameras, further enriching the downstream applications of hand motion forecasting.

REFERENCES

- [1] Ri-Zhao Qiu, Shiqi Yang, Xuxin Cheng, Chaitanya Chawla, Jialong Li, Tairan He, Ge Yan, Lars Paulsen, Ge Yang, et al. Humanoid policy” human policy. *arXiv preprint arXiv:2503.13441*, 2025.
- [2] Simar Kaireer, Dhruv Patel, Ryan Punamiya, Pranay Mathur, Shuo Cheng, Chen Wang, Judy Hoffman, and Danfei Xu. Egomimic: Scaling imitation learning via egocentric video. *arXiv preprint arXiv:2410.24221*, 2024.
- [3] Chen Wang, Haochen Shi, Weizhuo Wang, Ruohan Zhang, Li Fei-Fei, and C Karen Liu. Dexcap: Scalable and portable mocap data collection system for dexterous manipulation. *arXiv preprint arXiv:2403.07788*, 2024.
- [4] Andrea Bandini and José Zariffa. Analysis of the hands in egocentric vision: A survey. *TPAMI*, 45(6):6846–6866, 2020.
- [5] Mengmi Zhang, Keng Teck Ma, Joo Hwee Lim, Qi Zhao, and Jiashi Feng. Deep future gaze: Gaze anticipation on egocentric videos using adversarial networks. In *CVPR*, pages 4372–4381, 2017.
- [6] Bolin Lai, Miao Liu, Fiona Ryan, and James M Rehg. In the eye of transformer: Global-local correlation for egocentric gaze estimation and beyond. *IJCV*, 132(3):854–871, 2024.
- [7] Yin Li, Alireza Fathi, and James M Rehg. Learning to predict gaze in egocentric video. In *ICCV*, pages 3216–3223, 2013.
- [8] Yin Li, Miao Liu, and James M Rehg. In the eye of beholder: Joint learning of gaze and actions in first person video. In *ECCV*, 2018.
- [9] Debaditya Roy, Ramanathan Rajendiran, and Basura Fernando. Interaction region visual transformer for egocentric action anticipation. In *WACV*, pages 6740–6750, 2024.
- [10] Tushar Nagarajan, Yanghao Li, Christoph Feichtenhofer, and Kristen Grauman. Ego-topo: Environment affordances from egocentric video. In *CVPR*, pages 163–172, 2020.
- [11] Lorenzo Mur-Labadia, Ruben Martinez-Cantin, Josechu Guerrero, Giovanni Maria Farinella, and Antonino Furnari. Aff-attention! affordances and attention models for short-term object interaction anticipation. *arXiv preprint arXiv:2406.01194*, 2024.
- [12] Miao Liu, Siyu Tang, Yin Li, and James M Rehg. Forecasting human-object interaction: joint prediction of motor attention and actions in first person video. In *ECCV*, pages 704–721, 2020.
- [13] Shaowei Liu, Subarna Tripathi, Somdeb Majumdar, and Xiaolong Wang. Joint hand motion and interaction hotspots prediction from egocentric videos. In *CVPR*, pages 3282–3292, 2022.

[14] Wentao Bao, Lele Chen, Libing Zeng, Zhong Li, Yi Xu, Junsong Yuan, and Yu Kong. Uncertainty-aware state space transformer for egocentric 3d hand trajectory forecasting. In *ICCV*, 2023.

[15] Junyi Ma, Jingyi Xu, Xieyuanli Chen, and Hesheng Wang. Diffip2d: Diffusion-based hand-object interaction prediction on egocentric videos. In *IROS*, 2025.

[16] Junyi Ma, Xieyuanli Chen, Wentao Bao, Jingyi Xu, and Hesheng Wang. Madiff: Motion-aware mamba diffusion models for hand trajectory prediction on egocentric videos. *arXiv preprint arXiv:2409.02638*, 2024.

[17] Masashi Hatano, Ryo Hachiuma, and Hideo Saito. Emag: Ego-motion aware and generalizable 2d hand forecasting from egocentric videos. In *ECCVW*, 2024.

[18] Kailin Li, Puahao Li, Tengyu Liu, Yuyang Li, and Siyuan Huang. Maniptrans: Efficient dexterous bimanual manipulation transfer via residual learning. In *CVPR*, 2025.

[19] Junyi Ma, Wentao Bao, Jingyi Xu, Guanzhong Sun, Xieyuanli Chen, and Hesheng Wang. Novel diffusion models for multimodal 3d hand trajectory prediction. In *IROS*, 2025.

[20] Ashish Vaswani, Noam Shazeer, Niki Parmar, Jakob Uszkoreit, Llion Jones, Aidan N Gomez, Łukasz Kaiser, and Illia Polosukhin. Attention is all you need. *NeurIPS*, 30, 2017.

[21] Albert Gu and Tri Dao. Mamba: Linear-time sequence modeling with selective state spaces. *arXiv preprint arXiv:2312.00752*, 2023.

[22] Chen Bao, Jiarui Xu, Xiaolong Wang, Abhinav Gupta, and Homanga Bharadhwaj. Handsonvlm: Vision-language models for hand-object interaction prediction. *arXiv preprint arXiv:2412.13187*, 2024.

[23] Shikhar Bahl, Russell Mendonca, Lili Chen, Unnat Jain, and Deepak Pathak. Affordances from human videos as a versatile representation for robotics. In *CVPR*, pages 13778–13790, 2023.

[24] Masashi Hatano, Zhifan Zhu, Hideo Saito, and Dima Damen. The invisible egohand: 3d hand forecasting through egobody pose estimation. *arXiv preprint arXiv:2504.08654*, 2025.

[25] Georgios Pavlakos, Dandan Shan, Ilija Radosavovic, Angjoo Kanazawa, David Fouhey, and Jitendra Malik. Reconstructing hands in 3d with transformers. In *CVPR*, pages 9826–9836, 2024.

[26] Haoye Dong, Aviral Chharia, Wenbo Gou, Francisco Vicente Carrasco, and Fernando D De la Torre. Hamba: Single-view 3d hand reconstruction with graph-guided bi-scanning mamba. *NeurIPS*, 37:2127–2160, 2024.

[27] Mengcheng Li, Hongwen Zhang, Yuxiang Zhang, Ruizhi Shao, Tao Yu, and Yebin Liu. Hhmr: Holistic hand mesh recovery by enhancing the multimodal controllability of graph diffusion models. In *CVPR*, pages 645–654, 2024.

[28] Yating Tian, Hongwen Zhang, Yebin Liu, and Limin Wang. Recovering 3d human mesh from monocular images: A survey. *TPAMI*, 45(12):15406–15425, 2023.

[29] Jeongwan On, Kyeonghwan Gwak, Gunyoung Kang, Junuk Cha, Soohyun Hwang, Hyein Hwang, and Seungryul Baek. Bigs: Bi-manual category-agnostic interaction reconstruction from monocular videos via 3d gaussian splatting. In *CVPR*, 2025.

[30] Yufei Ye, Abhinav Gupta, and Shubham Tulsiani. What's in your hands? 3d reconstruction of generic objects in hands. In *CVPR*, pages 3895–3905, 2022.

[31] Yumeng Liu, Xiaoxiao Long, Zemin Yang, Yuan Liu, Marc Habermann, Christian Theobalt, Yuexin Ma, and Wenping Wang. Easyhoi: Unleashing the power of large models for reconstructing hand-object interactions in the wild. *arXiv preprint arXiv:2411.14280*, 2024.

[32] Zhifan Zhu and Dima Damen. Get a grip: Reconstructing hand-object stable grasps in egocentric videos. *arXiv preprint arXiv:2312.15719*, 2023.

[33] Jonathan Ho, Ajay Jain, and Pieter Abbeel. Denoising diffusion probabilistic models. *NeurIPS*, 33:6840–6851, 2020.

[34] Prafulla Dhariwal and Alexander Nichol. Diffusion models beat gans on image synthesis. *NeurIPS*, 34:8780–8794, 2021.

[35] Mengqi Zhang, Yang Fu, Zheng Ding, Sifei Liu, Zhuowen Tu, and Xiaolong Wang. Holdiffusion: Generating realistic 3d hand-object interaction data. In *CVPR*, pages 8521–8531, 2024.

[36] Keyang Zhou, Bharat Lal Bhatnagar, Jan Eric Lenssen, and Gerard Pons-Moll. Gears: Local geometry-aware hand-object interaction synthesis. In *CVPR*, pages 20634–20643, 2024.

[37] Sammy Christen, Shreyas Hampali, Fadime Sener, Edoardo Remelli, Tomas Hodan, Eric Sauser, Shugao Ma, and Bugra Tekin. Diffh2o: Diffusion-based synthesis of hand-object interactions from textual descriptions. In *SIGGRAPH Asia 2024 Conference Papers*, pages 1–11, 2024.

[38] Zichen Zhang, Hongchen Luo, Wei Zhai, Yang Cao, and Yu Kang. Pear: Phrase-based hand-object interaction anticipation. *arXiv preprint arXiv:2407.21510*, 2024.

[39] Bowen Tang, Kaihao Zhang, Wenhan Luo, Wei Liu, and Hongdong Li. Prompting future driven diffusion model for hand motion prediction. In *ECCV*, pages 169–186. Springer, 2024.

[40] Shanshan Gong, Mukai Li, Jiangtao Feng, Zhiyong Wu, and Lingpeng Kong. Diffuseq: Sequence to sequence text generation with diffusion models. In *ICLR*, 2023.

[41] Cheng Chi, Zhenjia Xu, Siyuan Feng, Eric Cousineau, Yilun Du, Benjamin Burchfiel, Russ Tedrake, and Shuran Song. Diffusion policy: Visuomotor policy learning via action diffusion. *IJRR*, 2023.

[42] Yanjie Ze, Gu Zhang, Kangning Zhang, Chenyuan Hu, Muhan Wang, and Huazhe Xu. 3d diffusion policy: Generalizable visuomotor policy learning via simple 3d representations. *arXiv preprint arXiv:2403.03954*, 2024.

[43] Suraj Nair, Aravind Rajeswaran, Vikash Kumar, Chelsea Finn, and Abhinav Gupta. R3m: A universal visual representation for robot manipulation. *arXiv preprint arXiv:2203.12601*, 2022.

[44] Arjun Majumdar, Karmesh Yadav, Sergio Arnaud, Jason Ma, Claire Chen, Sneha Silwal, Aryan Jain, Vincent-Pierre Berges, Tingfan Wu, Jay Vakil, et al. Where are we in the search for an artificial visual cortex for embodied intelligence? *NeurIPS*, 2023.

[45] Tete Xiao, Ilija Radosavovic, Trevor Darrell, and Jitendra Malik. Masked visual pre-training for motor control. *arXiv preprint arXiv:2203.06173*, 2022.

[46] Shraman Pramanick, Yale Song, Sayan Nag, Kevin Qinghong Lin, Hardik Shah, Mike Zheng Shou, Rama Chellappa, and Pengchuan Zhang. Egovlpv2: Egocentric video-language pre-training with fusion in the backbone. In *ICCV*, pages 5285–5297, 2023.

[47] Jinhan Li, Yifeng Zhu, Yuqi Xie, Zhenyu Jiang, Mingyo Seo, Georgios Pavlakos, and Yuke Zhu. Okami: Teaching humanoid robots manipulation skills through single video imitation. In *CoRL*, 2024.

[48] Huayi Zhou, Ruixiang Wang, Yunxin Tai, Yueci Deng, Guiliang Liu, and Kui Jia. You only teach once: Learn one-shot bimanual robotic manipulation from video demonstrations. *arXiv preprint arXiv:2501.14208*, 2025.

[49] Juntao Ren, Priya Sundaresan, Dorsa Sadigh, Sanjiban Choudhury, and Jeannette Bohg. Motion tracks: A unified representation for human-robot transfer in few-shot imitation learning. *arXiv preprint arXiv:2501.06994*, 2025.

[50] Chuan Wen, Xingyu Lin, John So, Kai Chen, Qi Dou, Yang Gao, and Pieter Abbeel. Any-point trajectory modeling for policy learning. *arXiv preprint arXiv:2401.00025*, 2023.

[51] Himangi Mittal, Nakul Agarwal, Shao-Yuan Lo, and Kwonjoon Lee. Can't make an omelette without breaking some eggs: Plausible action anticipation using large video-language models. In *CVPR*, pages 18580–18590, 2024.

[52] Zhaobo Qi, Shuhui Wang, Weigang Zhang, and Qingming Huang. Uncertainty-boosted robust video activity anticipation. *TPAMI*, 2024.

[53] Zeyun Zhong, David Schneider, Michael Voit, Rainer Stiefelhagen, and Jürgen Beyerer. Anticipative feature fusion transformer for multi-modal action anticipation. In *WACV*, pages 6068–6077, 2023.

[54] Antonino Furnari and Giovanni Maria Farinella. Rolling-unrolling lstms for action anticipation from first-person video. *TPAMI*, 43(11):4021–4036, 2020.

[55] Alexandros Stergiou and Dima Damen. The wisdom of crowds: Temporal progressive attention for early action prediction. In *CVPR*, pages 14709–14719, 2023.

[56] Junwu Weng, Xudong Jiang, Wei-Long Zheng, and Junsong Yuan. Early action recognition with category exclusion using policy-based reinforcement learning. *TCSVT*, 30(12):4626–4638, 2020.

[57] Toby Perrett, Alessandro Masullo, Tilo Burghardt, Majid Mirmehdi, and Dima Damen. Temporal-relational crosstransformers for few-shot action recognition. In *CVPR*, pages 475–484, 2021.

[58] Yin-Dong Zheng, Zhaoyang Liu, Tong Lu, and Limin Wang. Dynamic sampling networks for efficient action recognition in videos. *TIP*, 29:7970–7983, 2020.

[59] Yilong Wang, Zilin Gao, Qilong Wang, Zhaofeng Chen, Peihua Li, and Qinghua Hu. Tamt: Temporal-aware model tuning for cross-domain few-shot action recognition. *arXiv preprint arXiv:2411.19041*, 2024.

[60] Masashi Hatano, Ryo Hachiuma, Ryo Fujii, and Hideo Saito. Multimodal cross-domain few-shot learning for egocentric action recognition. In *ECCV*, pages 182–199. Springer, 2024.

[61] David G Lowe. Distinctive image features from scale-invariant keypoints. *International journal of computer vision*, 60:91–110, 2004.

[62] Martin A Fischler and Robert C Bolles. Random sample consensus: a paradigm for model fitting with applications to image analysis and automated cartography. *Communications of the ACM*, 24(6):381–395, 1981.

[63] Liunian Harold Li, Pengchuan Zhang, Haotian Zhang, Jianwei Yang, Chunyuan Li, Yiwu Zhong, Lijuan Wang, Lu Yuan, Lei Zhang, Jenq-Neng Hwang, Kai-Wei Chang, and Jianfeng Gao. Grounded language-image pre-training. In *CVPR*, pages 10965–10975, 2022.

[64] Alec Radford, Jong Wook Kim, Chris Hallacy, Aditya Ramesh, Gabriel Goh, Sandhini Agarwal, Girish Sastry, Amanda Askell, Pamela Mishkin, Jack Clark, et al. Learning transferable visual models from natural language supervision. In *ICML*, 2021.

[65] Chaoning Zhang, Dongshen Han, Yu Qiao, Jung Uk Kim, Sung-Ho Bae, Seungkyu Lee, and Choong Seon Hong. Faster segment anything: Towards lightweight sam for mobile applications. *arXiv preprint arXiv:2306.14289*, 2023.

[66] Yiming Li, Ziang Cao, Andrew Liang, Benjamin Liang, Luoyao Chen, Hang Zhao, and Chen Feng. Egocentric prediction of action target in 3d. In *CVPR*, pages 20971–20980, 2022.

[67] Daniel DeTone, Tomasz Malisiewicz, and Andrew Rabinovich. Deep image homography estimation. *arXiv preprint arXiv:1606.03798*, 2016.

[68] Taein Kwon, Bugra Tekin, Jan Stühmer, Federica Bogo, and Marc Pollefeys. H2o: Two hands manipulating objects for first person interaction recognition. In *ICCV*, pages 10138–10148, 2021.

[69] Prithviraj Banerjee, Sindi Shkodrani, Pierre Moulon, Shreyas Hampali, Shangchen Han, Fan Zhang, Linguang Zhang, Jade Fountain, Edward Miller, Selen Basol, et al. Hot3d: Hand and object tracking in 3d from egocentric multi-view videos. *arXiv preprint arXiv:2411.19167*, 2024.

[70] Dima Damen, Hazel Doughty, Giovanni Maria Farinella, Sanja Fidler, Antonino Furnari, Evangelos Kazakos, Davide Moltisanti, Jonathan Munro, Toby Perrett, Will Price, et al. Scaling egocentric vision: The epic-kitchens dataset. In *ECCV*, pages 720–736, 2018.

[71] Tony Z Zhao, Vikash Kumar, Sergey Levine, and Chelsea Finn. Learning fine-grained bimanual manipulation with low-cost hardware. *arXiv preprint arXiv:2304.13705*, 2023.

[72] Tianhe Ren, Shilong Liu, Ailing Zeng, Jing Lin, Kunchang Li, He Cao, Jiayu Chen, Xinyu Huang, Yukang Chen, Feng Yan, Zhaoyang Zeng, Hao Zhang, Feng Li, Jie Yang, Hongyang Li, Qing Jiang, and Lei Zhang. Grounded sam: Assembling open-world models for diverse visual tasks. *arXiv preprint arXiv:2401.14159*, 2024.

[73] Erhang Zhang, Junyi Ma, Yin-Dong Zheng, Yixuan Zhou, and Hesheng Wang. Zero-shot temporal interaction localization for egocentric videos. In *IROS*, 2025.

[74] Diederik P Kingma and Jimmy Ba. Adam: A method for stochastic optimization. *arXiv preprint arXiv:1412.6980*, 2014.

[75] Zihan Wang, Fanheng Kong, Shi Feng, Ming Wang, Han Zhao, Daling Wang, and Yifei Zhang. Is mamba effective for time series forecasting? *Neurocomputing*, 619:129178, 2025.

[76] Chen Wang, Fei Xia, Wenhao Yu, Tingnan Zhang, Ruohan Zhang, C Karen Liu, Li Fei-Fei, Jie Tan, and Jacky Liang. Chain-of-modality: Learning manipulation programs from multimodal human videos with vision-language-models. *arXiv preprint arXiv:2504.13351*, 2025.

[77] Javier Romero, Dimitrios Tzionas, and Michael J Black. Embodied hands: Modeling and capturing hands and bodies together. *arXiv preprint arXiv:2201.02610*, 2022.

[78] Zhe Cao, Tomas Simon, Shih-En Wei, and Yaser Sheikh. Realtime multi-person 2d pose estimation using part affinity fields. In *Proceedings of the IEEE conference on computer vision and pattern recognition*, pages 7291–7299, 2017.

[79] Shangchen Han, Po-chen Wu, Yubo Zhang, Beibei Liu, Linguang Zhang, Zheng Wang, Weiguang Si, Peizhao Zhang, Yujun Cai, Tomas Hodan, et al. Umetrack: Unified multi-view end-to-end hand tracking for vr. In *SIGGRAPH Asia 2022 Conference Papers*, pages 1–9, 2022.

Supplementary Material

A DATA ORGANIZATION FOR PUBLIC DATASETS

We follow the setups of the prior works [14], [19] to organize EgoPAT3D-DT, H2O-PT, and HOT3D-Clips datasets. For the video clips at 30 FPS in both EgoPAT3D-DT and H2O-PT, we follow the setup of USST [14], which splits the past and future sequences of each clip at the fixed ratio 60% by default. For HOT3D-Clips, we first downsample the video clips from 30 FPS to 10 FPS, and then also use 60% to split past and future sequences. Notably, the experiments on HOT3D-Clips only exclusively attend to the Aria part [19], as the Quest 3 part lacks RGB image streams. Besides, due to a lack of GT labels of its official test set, we partition its official training set into the training and test splits randomly in this work. As to our final splits of these public datasets, EgoPAT3D-DT contains 6356 training sequences with 1605 (seen scenes) and 2334 (unseen scenes) test sequences, while H2O-PT comprises 8203 training and 3715 test sequences. In HOT3D-Clips, we randomly sampled 2,732 training sequences and 300 test sequences, covering both left- and right-hand interactions.

B JOINT SELECTION FOR H2O-PT AND HOT3D-CLIPS

We select different joint combinations as prediction targets in the H2O-PT and HOT3D-Clips datasets. H2O-PT follows the MANO hand model [77] and captures 21 joint locations (the 15 original ones supplemented by 6 fingertip/wrist keypoints, to achieve compatibility with the OpenPose skeleton framework [78]. To validate that our proposed Uni-Hand can be adapted to different hand models, we attend to the hand annotations in the UmeTrack format [79] with 20 joint locations for HOT3D-Clips. Considering potential downstream tasks [49], we predict trajectories of five joints for these two datasets: one on the wrist and two each on the thumb and index finger, as shown in Fig. A. The joint indices for the MANO hand model in H2O-PT are [0, 1, 4, 5, 8]. The counterparts for the UmeTrack model in HOT3D-Clips are [0, 1, 5, 6, 8]. We refer to the original joint order in these two datasets. Fig. A(c) presents the exampled target indicators for HOT3D-Clips, which facilitates our Uni-Hand to understand different motion patterns of multiple target joints.

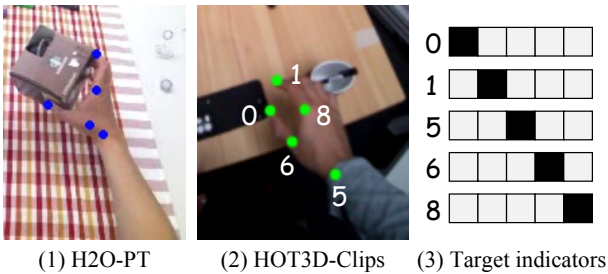


Fig. A: Visualization of prediction target joints of H2O-PT and HOT3D-Clips. We also illustrate the target indicators for HOT3D-Clips, which are one-hot embeddings introduced in Sec. 3.2.2 of the main text.

C HAND-GRIPPER POSE MAPPING

Our work attends to forecasting reasonable hand waypoints and interaction states, rather than fine-grained 3D hand-object interaction (HOI) analysis. Therefore, for all the robotic manipulation tasks in this benchmark, we manually curate the *point2pose* mapping from human hand grasp poses to robot grasp poses. Concretely, for all the manipulation tasks, we predict the trajectories of the wrist keypoint by the HMF method. Then we take the wrist keypoint as the anchor and map it to an ad-hoc gripper pose for pushing, picking, and placing. The rationale for constructing *point2pose* mapping lies in that the hand and the object basically satisfy a rigid connection in this benchmark, and the hand poses can be determined by the wrist positions during the push and pick-and-place periods. Another reason we predict the wrist in manipulation tasks is that the wrist is rarely occluded by the target object, whereas the finger joints tend to be obscured by the object during contact. This affects the annotation quality in our vision-only scheme of the HAT benchmark without any MoCap system. In the future, we will extend our proposed HAT benchmark to achieve learnable hand-gripper keypoint retargeting for more extensive robot tasks.

D ABLATION STUDY ON HYBRID ARCHITECTURES OF HMTM

In this section, we report Uni-Hand performance with multiple hybrid patterns of Mamba and Transformer in HMTM. Considering resource limitations in practical real-world deployments, we only evaluate the combinations of one/two egomotion-aware Mamba (EAM) blocks and one structure-aware Transformer (SAT) here. As shown in Tab. A, versions 5 and 3 achieve more accurate hand waypoint predictions than version 4. This suggests that stacking EAM blocks sequentially enhances hand-state modeling compared to the case where EAM blocks are separated by SAT. Additionally, version 5 and version 2 generally outperform version 3 and version 1 respectively in 3D-space evaluations, which presents the posterior Transformer module's positive impact on forecasting performance. This suggests that the preceding EAM blocks provide clean temporal feature representations for the following global context fusion, and the subsequent SAT facilitates global refinement for temporal modeling results through cross-attention mechanisms.

In addition, we ablate the EAM-EAM-SAT combos of Uni-Hand by replacing its EAM blocks with LSTM and the vanilla Transformer (VT) on H2O-PT. Tab. B shows that the egomotion-aware Mamba significantly outperforms LSTM and VT. This indicates that EAM effectively models temporal hand motion features within both past observations and future predictions. Compared to LSTM and VT, the devised motion-driven selective scan incorporates camera egomotion trends to achieve reasonable hand state transitions in temporal modelling.

E ABLATION STUDY ON AUTO-TIL

In Sec. 4.1.3 of the main text, we propose labelling the GT interaction states for our HAT benchmark in two ways:

TABLE A: Comparison of performance on hand trajectory prediction on different hybrid patterns of the EAM and SAT blocks in the hybrid Mamba-Transformer module of Uni-Hand. Here we report ADE and FDE in 3D space/2D projection space following [15]. Best and secondary results are viewed in **bold black** and **blue** colors.

Version	Hybrid pattern	EgoPAT3D-DT (seen)		EgoPAT3D-DT (unseen)		H2O-PT	
		ADE \downarrow	FDE \downarrow	ADE \downarrow	FDE \downarrow	ADE \downarrow	FDE \downarrow
1	SAT-EAM	0.184/0.076	0.353/0.117	0.147/0.066	0.236/0.100	0.033/0.042	0.057/0.050
2	EAM-SAT	0.177/ 0.072	0.345/ 0.116	0.133/ 0.063	0.217/ 0.098	0.031 /0.042	0.054/0.048
3	SAT-EAM-EAM	0.173 /0.073	0.339 / 0.113	0.132 /0.064	0.198 / 0.098	0.030 / 0.037	0.051 / 0.039
4	EAM-SAT-EAM	0.226/0.151	0.402/0.207	0.181/0.135	0.266/0.186	0.031 / 0.038	0.053/ 0.045
5	EAM-EAM-SAT	0.170 / 0.071	0.336 /0.118	0.118 / 0.061	0.189 / 0.099	0.030 / 0.037	0.050 / 0.039

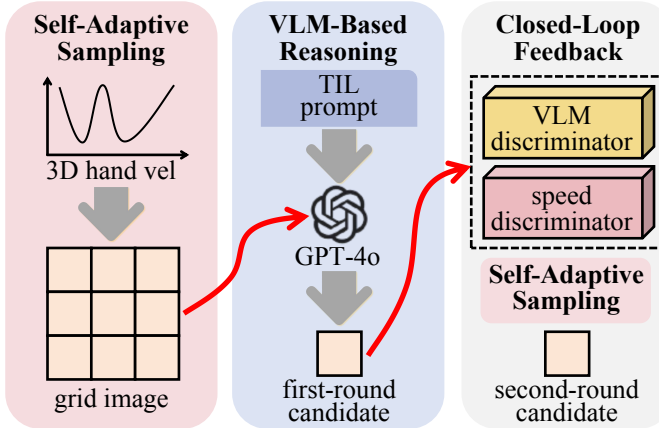


Fig. B: High-level diagram of EgoLoc, the SOTA TIL approach developed by Zhang *et al.* [73].

TABLE B: Ablation study on egomotion-aware Mamba. Here we report ADE and FDE in 3D space/2D projection space following [15]. Best results are viewed in **bold black**.

Approach	ADE \downarrow	FDE \downarrow
LSTM	0.045/0.051	0.078/0.069
VT	0.036/0.046	0.062/0.060
EAM	0.030 / 0.037	0.050 / 0.039

(1) manual annotation, and (2) automated temporal interaction localization (auto-TIL) using EgoLoc [73], which are ablated here with the robotic manipulation task of “put the block onto the cloth”. Fig. B illustrates the high-level diagram of EgoLoc for fine-grained interaction localization. EgoLoc first adaptively samples key frames from the input video clip according to hand velocities, leading to a grid image as the visual prompt for the following VLM-based reasoning. Subsequently, prompted with an additional TIL text prompt, GPT-4o is utilized to localize the timings of hand-object contact and separation. The first-round image candidate is further verified by the closed-loop feedback mechanism. Two devised discriminators decide whether to resample from the input video and output the ultimate second-round candidate. Auto-TIL by EgoLoc does not require any manual intervention to label the hand-object contact/separation timings, leading to interaction state annotations $\mathcal{G}^f = \{G_t\}_{t=1}^{N_f} (G_t \in \{0, 1\})$. We report the ADE and FDE metrics in 3D on the validation sets and the success rates of 10 test trials. As shown in Tab. C, auto-TIL can still reasonably supervise Uni-Hand to complete the test trials with a success rate of 70%. This suggests that it can generate reasonable trajectory planning, although it holds greater

TABLE C: Ablation study on GT interaction states. We present the errors of hand trajectory prediction and interaction state prediction on the validation set, as well as the success rates (SR) of the test trials for “put the block onto the cloth”. Best results are viewed in **bold black**.

Approach	ADE \downarrow	FDE \downarrow	MAE \downarrow	SR \uparrow
Auto-TIL	0.067	0.088	3.5	70%
Manual	0.035	0.012	1.9	90%

errors on the validation sets. Considering that the GT hand waypoints are also labelled by HaMeR [25] automatically, we present that our proposed paradigm has the potential to automatically parse human activity videos, optimize effective motion forecasting models, and transfer them to robotic platforms to implement manipulation tasks. That is, it shows strong potential for scaling up with unlabeled human motion data.

F STUDY ON PRETRAINING WITH PUBLICLY AVAILABLE DATASETS

We further explore how pertaining with public datasets affects Uni-Hand’s ability to facilitate downstream robotic manipulation. We organize a combination of the training sets from EgoPAT3D-DT, H2O-PT, and HOT3D-Clips. After pretraining Uni-Hand with the dataset combos, we exploit the weights to initialize the Uni-Hand model that will be fine-tuned by our HAT benchmark. The new TAT module is appended after the pretrained SAT module, since the pretraining process does not involve task-specific prompts. Note that we fine-tune the weights of all the modules of Uni-Hand for the task “put the block onto the cloth”. As shown in Tab. D, pretraining with large-scale public hand motion data generally reduces hand trajectory prediction errors, but increases the errors in interaction state prediction. This indicates that the pretraining operation facilitates human-like trajectory planning for robotic manipulation. However, it cannot improve the optimization of finding hand-object contact/separation timings, as such annotations are absent in the pretraining combos.

G PREDICTION ERRORS OVER TIME

Here we further report the temporal variation of prediction errors in our HAT benchmark. Fig. C shows the error trend of one randomly sampled validation case in each task. As can be seen, the prediction error tends to be lower around

TABLE D: Study on pretraining with publicly available datasets. We present the errors of hand trajectory prediction and interaction state prediction on the validation set (20 out of the training samples)/test trials, as well as the success rates (SR) of “put the block onto the cloth”. Best results are viewed in **bold black**.

Approach	ADE \downarrow	FDE \downarrow	MAE \downarrow	SR \uparrow
Vanilla	0.035/0.050	0.012/0.019	1.8/2.4	90%
Pretrained	0.033/0.046	0.012/0.019	2.4/2.5	90%

the timings of hand-object contact. This suggests that hand demonstrations hold lower uncertainties at these timings thanks to precise pick requirements, leading to more stable supervision signals to optimize Uni-Hand. This trend also facilitates plausible action planning despite relatively higher errors at other timings (e.g., the initial stage).

H GENERALIZABILITY ASSESSMENT

In Sec. 4.3 of the main text, we have demonstrated Uni-Hand’s strong generalization ability to unseen environments in the publicly available dataset. Here we further present its generalizability with respect to the robot pick-and-place task. We train Uni-Hand with the recorded data of the language-conditioned task “put the blue block onto the cloth”, where the target block is cube-shaped. Then we deploy the pretrained model to the same task but with a block of a different shape. As shown in Fig. D(a), the novel cuboid-shaped block is formed by bonding two cubic blocks together. In this experiment, we achieved a 60% success rate, and one successful case is illustrated in Fig. D(b). This demonstrates that Uni-Hand generalizes well to objects with different shapes in the language-conditioned manipulation task. This good generalizability likely stems from the utilization of point clouds and the injection of task-aware text embeddings. We leave the generalizability assessment using objects with more diverse shapes as our future work.

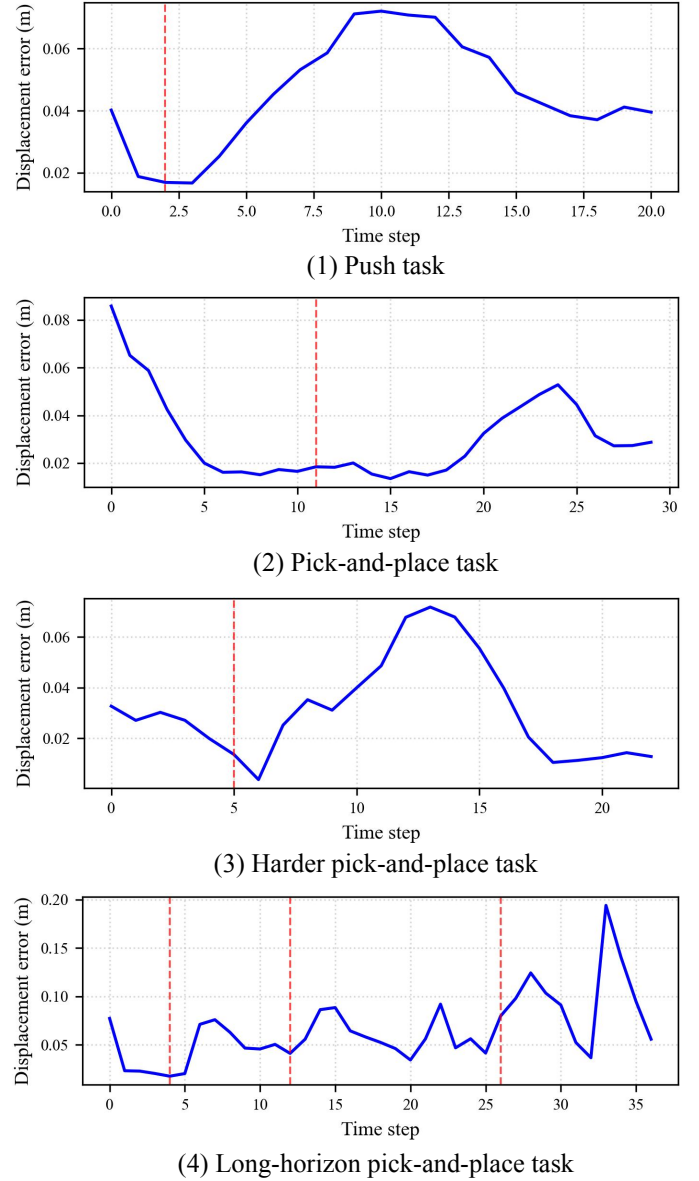


Fig. C: Temporal variation of prediction errors. We illustrate the displacement errors between GT hand waypoints and predicted counterparts (blue solid lines), as well as predicted hand-object contact timings (red dashed lines).

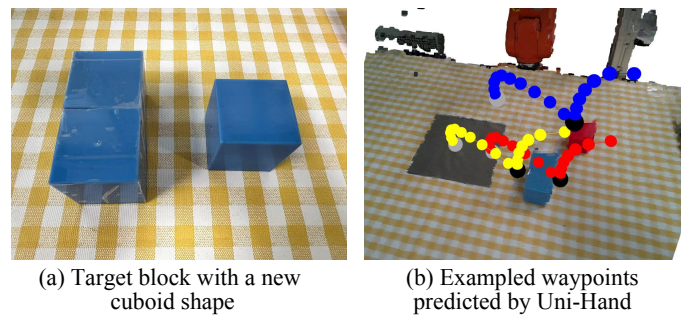


Fig. D: Generalizability assessment in the robotic language-conditioned manipulation.